Title: HMG box-containing protein 1 (HBP1) prevents pancreatic injury in experimental pancreatitis but accelerates pancreatic neoplasia progression.

Short title:

Authors: Seung-Won Lee*[1], Taelor Ekstrom*[1], Elise C. Manalo[1], Shangyuan Ye[3], Mark Berry[1], Dmytro Grygoryev[1], Malwina Szczepaniak[1], Carlos Origel Marmolejo[1], Syber Haverlack[1], Jinho Lee[4, 5], Vidhi M. Shah[2,6], Dove Keith[6], John L. Muschler[6,7,8], Koei Chin[1,8], Rosalie C Sears[2,6,7], Stuart P. Weisberg[9], Terry Morgan[1, 7, 10], Jungsun Kim[1,2,7,11]

[1]Cancer Early Detection Advanced Research Center, Knight Cancer Institute, Oregon Health & Science University (OHSU), School of Medicine, Portland, OR.
[2]Department of Molecular and Medical Genetics, OHSU School of Medicine, Portland, OR.
[3]Biostatistics Shared resource, Knight Cancer Institute, OHSU School of Medicine, Portland, OR.
[4]Division of Oncologic Sciences, Knight Cancer Institute, OHSU School of Medicine, Portland, OR.
[5]Knight Diagnostic Laboratories, OHSU School of Medicine, Portland, OR.
[6]Brenden-Colson Center for Pancreatic Care, OHSU school of medicine, Portland, OR.
[7]Cancer Biology Program, Knight Cancer Institute, OHSU School of Medicine, Portland, OR.
[8]Department of Biomedical Engineering, OHSU School of Medicine, Portland, OR.
[9]Department of Pathology, Columbia University Irving Medical Center, New York, NY
[10]Department of Pathology, OHSU School of Medicine, Portland, OR.
[11]Lead Contact

*Equal contribution

Grant Support: The work was funded by the MRF New Investigator Grant (GCNCR1042A to JK), National Pancreas Foundation (ACNCR1570 to JK), OHSU pilot grant, and Knight CEDAR (68182-947-000, 68182-976-000, and 68182-907-986) from the Cancer Early Detection Advanced Research Center at OHSU Knight Cancer Institute.

Abbreviations:

- Acute pancreatitis (AP)
- Chronic pancreatitis (CP)
- Fine-Needle Aspiration (FNA)
- Pancreatic ductal adenocarcinoma (PDAC)
- Pancreatic intraepithelial Neoplasia (PanIN)
- Intraductal Papillary Mucinous Neoplasm (IPMN)
- Intraductal papillary mucinous carcinoma (IPMC)
- Acinar-to-ductal metaplasia (ADM)
- HMG-box transcription factor 1 (HBP1)
- Cholecystokinin (CCK)
- Transcription factor (TF)
- Immunofluorescence (IF)
- immunohistochemistry (IHC)
- Hematoxylin & Eosin (H&E)
- Tissue microarray (TMA)
- Quantitive reverse transcription-PCR (qRT-PCR)
- Conditional knockout (CKO)
- Receiver operating characteristic (ROC)
- Area Under Curve (AUC)
- Regenerating gene (Reg)
- Uniform Manifold Approximation and Projection for Dimension Reduction (UMAP)
- Differentially regulated genes (DEG)

Correspondence: Jungsun Kim, Ph.D., 2720 SW Moody Ave., Portland, OR 97201. kimjungs@ohsu.edu. Office:503-346-1967.

Disclosures: The authors declare no potential conflicts of interest.

Transcript Profiling: Spatial Transcriptomic data is available on NCBI GSEx. Detailed analysis is available in the supplementary information. Additional results are available in supplementary figures and tables as resource datasets.

Writing Assistance: This manuscript was edited by Life Science Editors.

Author contributions: Conceptualization, JK; Investigation, TE, SWL, ECM, MB, DG, SH, JL, SY, JLM, KC, TM, SPW, JK; Formal Analysis, TE, SWL, ECM, MB, DG, SH, JL, SY, JLM, KC, TM, SPW, and JK; Data curation, SWL, DG, SY, and TM; Methodology, TE, SWL, ECM, MB, DG, SH, JL, VMS, JLM, KC, LF; Resource, VMS, DK, JLM, RCS; Writing, SWL and JK; Supervision, KC, RCS, and JK; Funding Acquisition, JK.

Data Transparency Statement: All data and analytic methods will be made available to other researchers. Further information about code and any requests can be directed to and will be fulfilled by the lead contact, Jungsun Kim (kimjungs@ohsu.edu).

ABSTRACT (260 words)

Background & Aims: Pancreatitis is an inflammatory disease of the exocrine pancreas and is a known risk factor for pancreatic ductal adenocarcinoma (PDAC). We previously identified HMG-box transcription factor 1 (HBP1) as a potential master transcription factor (TF) involved in the early progression of PDAC and associated with poor patient survival. However, the functional role of HBP1 in the pathophysiological mechanism for progression from acute to chronic pancreatitis to PDAC remains unclear.

Methods: We examined HBP1 expression in human chronic pancreatitis samples and cerulein-induced acute pancreatitis mouse model. We generated mice with pancreatic-specific conditional HBP1 knockout, without or with an oncogenic Kras mutation, and their corresponding controls. Then, we employed spatial proteomic and transcriptomics, histology, and immunostaining to characterize pathological changes in these mice. We validated findings from mouse models using inducible HBP1-overexpressing human pancreatic ductal epithelial cells.

Results: HBP1 was upregulated in pancreatic acinar cells in human chronic and mouse acute pancreatitis, and the expression of HBP1 in human chronic pancreatitis was associated with the presence of PDAC. Ablation of HBP1 in the pancreas disrupted acinar homeostasis by impairing the autophagic influx and exacerbated inflammation upon injury. However, in the presence of an oncogenic KRAS, HBP1 ablation delayed the formation of pancreatic intraepithelial neoplasia (PanINs), precursors of PDAC, and their progression into higher grades.

Conclusions: Upregulated HBP1 in normal acinar cells limits pancreatic inflammatory injury, but HBP1 is essential for PanIN progression in the presence of an oncogenic KRAS. Thus, HBP1 is a key regulator in both pancreatitis and early neoplastic changes and a potential target for therapeutic intervention in pancreatitis and PanIN progression.

Keywords (4-5): HMG box-containing protein 1 (HBP1), pancreatic injury, PanINs initiation, pancreatitis, and autophagy

Introduction (max 7000 words including main text; reference;table/figure legends)

Pancreatitis is an inflammatory disease of the exocrine pancreas caused by damaging acinar cells, which results in autodigestion, inflammation, and necrosis[1-6]. Although most patients with pancreatitis experience mild to moderately severe symptoms that resolve within days or weeks, approximately 20% of patients have a severe disease that can be lethal[1-5]. Recurrent acute pancreatitis (AP) can lead to chronic pancreatitis (CP), which is predisposed to developing pancreatic cancer[4]. However, the relationship between severe AP and the onset of CP is not linear. Therefore, a deeper understanding of factors and processes regulating pancreatitis is needed in order to better predict the outcome of pancreatitis and the progression of pancreatitis to pancreatic cancer[1-5].

Pathologically, mild AP is defined as when exocrine compartments display interstitial edema with a focal increase of immune cells but do not show any acinar drop-out, moderately severe AP is categorized if acinar dropout is focally seen along with infiltrating immune cells, and severe AP is classified if diffused (multifocal) acinar drop-outs are seen together with intensive infiltration of immune cells or chronic pancreatitis[5, 7, 8]. Thus, pathophysiologically, AP can be divided into two main types[5]: i) mild interstitial edematous pancreatitis that occurs in most patients and resolves within the first week and ii) severe necrotizing pancreatitis that is seen in 5-10% of patients. Interstitial edematous pancreatitis is characterized by homogeneous enlargement of the pancreatic parenchyma, due to inflammatory edema, along with mild inflammation of peripancreatic fat but without recognizable tissue necrosis. In contrast, necrotizing pancreatitis involves inflammation associated with both parenchymal and peripancreatic necrosis[5].

Several factors can induce and exaggerate pancreatitis. Premature activation of pancreatic enzymes leads to pancreatic injury, including pancreatic cell death, and triggers inflammation. Autophagy occurs in normal pancreatic acinar tissue to maintain its homeostasis[9]. Autophagy flux involves the entire sequence of autophagic events, from the initiation of autophagosome formation to autophagosome fusion with lysosomes and to lysosomal

degradation. Defects in the autophagy flux disrupt the acinar homeostasis, resulting in aberrant pancreatic cell death. A significant feature of AP is impaired autophagy flux, which is evidenced by the accumulation of large autophagic cell vacuoles decorated by p62 and LC3-II autophagosome markers in acinar cells[9]. The presence of an unresolved inflammatory response exacerbates the severity of pancreatitis[9-11].

For inducing pancreatitis experimentally, repeated intraperitoneal injections of cerulein are the most widely used and reproducible method[12-14]. Cerulein stimulates acinar cells to produce excessive digestive enzymes as well as inappropriate secretion of pancreatic enzymes and production of reactive oxygen species that induce inflammation and acinar cell death[12-14]. Similar to human AP, cerulein treatment induces histological changes, such as interstitial edema, leukocyte infiltration, and acinar cell dropout, that peak at 3-6 hours post-treatment. These changes begin to resolve by 24 hours, with the pancreas appearing morphologically normal after one week[15]. Prolonged cerulein treatment, especially in combination with the expression of an oncogenic Kras mutant, can lead to CP-like features, including persistent acinar atrophy, inflammation, and stabilized acinar-to-ductal metaplasia (ADM). This progression can further lead to pancreatic intraepithelial neoplasia (PanINs), the most common precursor to pancreatic ductal adenocarcinoma (PDAC)[14-17].

HMG-box transcription factor 1 (HBP1) regulates the G1-to-S cell cycle progression through binding RB[18-21]. Upregulated HBP1 induces senescence[22-24] and ferroptosis[25] and promotes DNA-break repair[26] upon oxidative stress or oncogenic mutations. Thus, HBP1 has traditionally been considered as a tumor suppressor. Yet, recent studies suggest that HBP1 may also function as a tumor promoter[27, 28] and that HBP1 serves as a hub across multiple signal pathways through various post-translational modifications[23, 25, 26, 29-32]. The role of HBP1, therefore, may be tissue- and context-dependent. We previously identified HBP1 as a potential master transcription factor (TF) in the early progression of PDAC and correlated its expression with poor patient survival[33]. We have also shown that HBP1 is expressed only in islet cells of adult normal

pancreata but it is expressed in exocrine cells in PDAC and in CP adjacent to PDAC in human[33]. Despite these findings, the functional role of HBP1 in pancreatitis and in the initiation of PanINs has not been reported. Herein, we investigated the role of HBP1 in AP and in the initiation and progression of PanINs.

MATERIALS and METHODS (1000 words-ish)

Mouse Model. All animal works were performed with the approval of the Institutional Animal Use and Care Committee (IACUC) of the OHSU (IP00004592). p48^{cre} (JAX stock #023329)[34] and LSL-K-ras$^{G12D/+}$ (JAX stock #008179)[35] mice were obtained from Jackson Laboratories and backcrossed onto the C57Bl/6J background. Hbp1$^{flox/flox}$ mice in the C57BL/6J and ICR backgrounds were recovered from cryopreserved 2-cell stage embryos, gifts from Dr. Ohtsuka's lab[36] as described[37]. Hbp1$^{flox/flox}$ mice have backcrossed at least five generations with p48^{Cre} C57Bl/6J mice (Fig. S2A). Transgenic genotypes were verified from tail genomic DNA using regular PCR or real-time PCR by Transnetyx (Table S1). Pancreatitis was induced in 8–10-week-old mice by seven hourly intraperitoneal injections of 50µg/kg body weight Cerulein (Sigma) as previously described[38], and pancreata were harvested 1, 2, and 7 days after the last Cerulein injection.

To generate p48^{Cre}; LSL-Kras^{G12D}; Hbp1$^{flox/flox}$ (Hbp1-null KCH: KCH Homozygous) or p48^{Cre}; LSL-Kras^{G12D}; Hbp1$^{wt/flox}$ (Hbp1-competent KCH: KCH heterozygous), we crossed Hbp1$^{flox/flox}$ mice with p48^{Cre}; LSL-Kras^{G12D} (Kras Cre mice: Hereinafter KC mice) mice. Pancreata at each of three-time points (10, 20, and 40 weeks old) to obtain i) body and pancreatic weights, ii) pancreatic tumor volumes, and iii) liver, lung, and local lymph node tumor burdens.

Human pancreatitis Tissue Microarray (TMA). De-identified human pancreatitis tissues were obtained under the Oregon Pancreas Tissue Registry study (IRB00003609). Informed consent was obtained from all subjects. The OHSU Institutional Review Board approved all experimental

protocols. All methods were carried out following relevant guidelines and regulations. Chronic pancreatitis tissues were harvested from fine-needle aspiration (FNA) or Whipple surgery of patients with intraductal papillary mucinous neoplasm (IPMN). Chronic pancreatitis tissues associated with tumors were harvested from the margin tissue of PDAC or Intraductal papillary mucinous carcinoma (IPMC) resections. TMA consists of six different pancreatitis areas from 49 patients with chronic pancreatitis (a total of 270 cores for pancreatitis). A total of 16 non-pancreatic tissues, such as the spleen, tonsil, and placenta, from the same patients were used as controls.

Nanostring's digital spatial profiling (DSP) GeoMx platform. Mouse immune cell profiling core, immune activation status, immune cell typing and immune-oncology drug target protein modules[39] were used. Briefly, after incubating panels for the pancreata of two HBP1 WT and two CKO mice each time after cerulein treatment day 1 and 2) with Pan-Cytokeratin (PanCK, for pancreatic epithelial cells) and CD45 (immune markers), a total of 96 regions of interest (ROI) with phenotypical pancreatitis were selected for the DSP analysis. UV-cleaved unique DNA oligos were collected and hybridized with fluorescent codesets for the molecule counts. The nCounter data were normalized using the geometric mean of all targets. We first computed the "signal-to-noise ratio (SNR) per target protein with IgG control values and selected 27 immune markers with higher than 1.6 SNR across all samples for downstream analysis. Normalized Geomean of nCounter is used for clustering and statistical analysis.

10x Visium Spatial Transcriptome: Spatial transcriptomic analysis was performed according to the manufacturer's instructions in the pancreata of two HBP1 WT and two HBP1 CKO mice at 24 and 48 hrs after cerulein treatment. Briefly, the pancreatitis areas were mounted on the 10x genomics Visium slide, with 5000 barcoded 55 µm size spots capturing 1 to 10 cells where each spot has millions of 20873 probes corresponding to 20,551 mouse genes[40], using CytAssist. After sequencing with 25k read pairs/spot, raw data was converted to FASTQ to map to H&E images

and feature-barcode matrices using Spaceranger for downstream analysis. Seurat packages were used to process, analyze, and visualize data[41], and the Harmony algorithm was used to correct technical variations among slides[42].

Statistical analysis for pancreatitis TMA: The HBP1 expression as measured by IF staining of the TMAs was summarized using the H-score as a function of the strength of staining (0=negative, 1=weak, 2=moderate, 3=strong). The percent of cells for that intensity was computed in each cell type using QuPath. To yield a continuous score for each cell type, each H-score was further multiplied by the percent of cells staining (0-100%) for that intensity and divided by 100, which can range from 0-3 for each cell type stained. Since each patient sample has a mixture of cell types, we further combined all scores of each cell type for each patient. We fitted a logistic regression model to see whether HBP1 expression levels in each cell type or combined cell types are associated with the presence of pancreatic tumors (PDAC+IPMC). Scores of each cell type are used as predictors, and the presence of a tumor is used as the outcome variable. To investigate the prediction power of the fitted model, we generated the ROC curve for the fitted model.

General Statistical Analysis Animals were age and sex-matched in each experiment. To compute statistical significance, we checked the data distribution using GraphPad Prism. Welch's unequal variances t-test and Mann-Whitney test are used for pair-wise comparison of normally and non-normally distributed data, respectively. A two-part fitted model was used for Fig. 2G due to the large proportion of zero observations in the dataset. The differences were considered statistically significant when p-values were below 0.05. A hypergeometric probability test determined if the observation was over random chance. Benjamin-Hochberg's procedure determined the false discovery rate (FDR). The reproducibility of molecular signatures was assessed using Spearman's rank correlation coefficient (ρ).

Tissue immunofluorescence (IF), immunohistochemistry (IHC), Hematoxylin and eosin (H&E), and Quantitative reverse transcription-PCR (qRT-PCR): All these protocols are described in detail in Supplementary Experimental Procedures.

RESULTS.

The expression of HBP1 is increased in pancreatitis and is associated with the pancreatitis progression. To investigate the potential role of HBP1 in the pathophysiological progression of pancreatitis and PanINs, we ascertained HBP1 expression in mouse cerulein-induced AP and human pancreatitis tissues using a verified HBP1 antibody (Fig. 1A and S1). In mice, HBP1 was scarce in normal pancreatic exocrine cells (Fig. 1B) but was widely increased in damaged pancreatic acinar cells after the cerulein treatment, reaching the maximum at 48 hours after the final cerulein treatment (Fig. 1C-D). Concurrent with the recovery from injury, the HBP1 protein disappeared by day 7 after cerulein treatment (Fig. 1E). These results indicated that the HBP1 expression increased during cerulein treatment-induced pancreatitis and correlated with its kinetics.

In human tissues, HBP1 was barely or only weakly expressed in normal acinar tissues, stroma, and other normal tissues (Fig. 1F-G) but was strongly expressed in injured acinar and ductal cells in pancreatitis tissues (Fig. 1H-K). To investigate whether the HBP1 level in pancreatitis tissues was associated with the presence of invasive tumor, we fitted a logistic regression model using tumor presence as the outcome variable and HBP1 expression levels in three cell types (fibroblast, acinar, and ductal) as predictors (See method). The analysis revealed that the HBP1 expression in fibroblast cells was significantly and negatively associated with the presence of tumor, suggesting a potential protective role. In contrast, HBP1 expressions in acinar and ductal cells showed negative and positive, respectively, but statistically non-significant

associations, possibly due to a more complex role of these compartments in the disease progression or insufficient sample sizes (Fig. S1J-K)

Next, we assessed whether HBP1 expression levels from individual cell types or all three cell types combined could differentiate pancreatitis patients with invasive tumors from those without tumors using receiver operating characteristic (ROC) curve analysis. The area under the ROC curve (AUC) values were 0.686 (95% CI: 0.4979-0.8741), 0.5899 (95% CI: 0.3932-0.7866), and 0.812 (95% CI: 0.6755-0.9625) for acinar, ductal, and stromal, respectively, whereas it was 0.865 (95% CI: 0.735-0.995) for three cell types combined, showing improved performance than any individuals (Fig. 1M). We included gender and age information in the fitted model, but neither variable is significant in all models (p-values=0.55 and 0.19, respectively).

In summary, HBP1 is ectopically overexpressed in cerulein-induced mouse AP and human CP tissues, and its expression in human CP is associated with the presence of invasive tumors within pancreatitis.

Loss of Hbp1 in the pancreas shows a grossly normal phenotype but exacerbates the AP severity. To investigate the pathophysiological functions of HBP1 during pancreatic inflammation and regeneration, we generated pancreatic-specific Hbp1 conditional knockout ("CKO") mice by crossing Hbp1$^{flox/flox}$ mice[36] with p48^{Cre} mice, in which Ptfl1a (p48)-Cre recombinase is expressed specifically in pancreatic progenitor and adult acinar cells[43] (HBP1 CKO mice: p48^{Cre}; Hbp1$^{flox/flox}$) (Fig. S2A-B, Table S1). Hbp1$^{flox/flox}$ mice were used as littermate wild type (WT) controls (HBP1 littermate WT control mice: Hbp1$^{flox/flox}$). Both sexes of HBP1 CKO mice developed normally and were born at expected Mendelian ratios with normal histology indistinguishable from control mice. We verified that HBP1 CKO mice had decreased expression of HBP1 in the pancreatic islet compartment (Fig. S2C-I).

.To assess the *in vivo* function of HBP1 in pancreatic injury and regeneration, we induced cerulein-mediated pancreatitis in HBP1 CKO and littermate control WT mice (Fig. 2A). Cerulein

treatments had minimal impact on the body weight in both groups yet increased normalized pancreatic weights compared to PBS treatment one-day after, reflecting edematous AP (Fig. 2B-C, Table S3A-C). The normalized pancreatic weights of HBP1 WT and CKO mice were not different on day 1 but those of HBP1 CKO mice were significantly lower than those of HBP1 WT control mice by day 2, indicating parenchymal destruction/atrophy that was often associated with severe pancreatitis (Fig. 2B-C, Table S3A-C).

Pancreatitis, determined by a pathologist based in a blinded manner on H&E staining images[5], occur at a higher frequency in HBP1 CKO mice than in control mice upon cerulein treatments (Fig. 2D-E). Because we did not observe any apparent associations of sex and age with the pancreatic injury, we did not include sex and age as adjustor variables in subsequent modeling analyses (Table. S3B-C).

Next, we assessed the severity of pancreatitis in the pancreata of HBP1 WT and CKO mice based on H&E staining images[5] (Fig. 2F). The exocrine compartments of cerulein-treated HBP1 WT mice displayed mild injury with degranulated acinar cells and interstitial edema. In contrast, those of cerulein-treated HBP1 CKO mice showed diffuse and more acinar dropout, indicating significantly increased severity of AP (Fig. 2E-G). As expected[15], the pancreas of both HBP1 control and CKO mice was repaired with regenerated acinar cells, and the morphology was indistinguishable from that of PBS-treated animals seven days after cerulein treatments (Fig. 2E, G). Because we use a Cerulein treatment condition for mild AP, we did not see a significant increase in the ADM population in either HBP1 WT or CKO mice (Fig. S2J).

Collectively, these data indicate that HBP1 protects the pancreata from initial pancreatic injury and fibrosis but is dispensable for pancreatic metaplasia, regeneration and resolution of inflammation.

Loss of HBP1 increases inflammation that is largely driven by macrophages in AP. HBP1 ablation increased pancreatic injury, we sought to identify leukocytes that differentially infiltrated

the pancreata of HBP1 CKO mice after cerulein treatment. Because contaminations by leukocytes from lymph nodes during tissue dissociation could exaggerate the extent of leukocytes infiltrating the pancreata when using flow cytometry, we used the DSP GeoMx platform with mouse immune cell panels[39] to spatially resolve cellular components (Fig. 3A). Pancreatic cores from HBP1 WT and CKO mice exhibited distinct clustering (Fig. 3B). Consistent with a prior report[44], HBP1 CKO pancreata showed increased Ki67, GAPDH, and CD45 (Fig. 3C). Importantly, HBP1 CKO pancreata had significantly increased myofibroblast (Fibronectin, SMA) and myeloid lineage (CD11b, F8/40, CD44 and VISTA) populations but had decreased T-cell tolerance signals (OX40L, CD4 and FoxP3) on days 1 and 2 after cerulein treatment (Fig. 3D-E, S3A-C).

To better spatially resolve leukocytes in the pancreatic inflammation, we performed IF with markers of T cells (CD3, CD4, CD8) and macrophages (F4/80). The infiltration of F4/80$^+$ macrophages into the pancreatic parenchyma was markedly higher in HBP1 CKO compared to control mice at days 1 and 2 after cerulein treatment whereas there was no detectable T cell infiltration into the pancreatic parenchyma during this period in these mice (Fig. 3F). In both groups, we observed marked accumulation of CD4$^+$ T cells in the center of peripancreatic lymph nodes with a dense rim of F4/80$^+$ macrophages around the periphery of the lymph nodes on days 1 and 2 after cerulein treatment (Fig. S4C). These results show that the increased inflammation in pancreatic parenchyma of HBP1 CKO mice during cerulein-induced pancreatitis is largely macrophage-driven, whereas T cells and macrophages accumulate in the peripancreatic lymph nodes similarly in the HBP1 WT and CKO mice.

Loss of HBP1 impairs pancreatic protection upon stress but increases immune response gene programs in AP. We hypothesized that HBP1 ablation may trigger the infiltration of macrophages by disrupting the acinar homeostasis upon injury by cerulein treatments. To understand how HBP1 ablation impaired acinar homeostasis and triggered the infiltration of macrophages, we characterized the spatial transcriptomics of the pancreas of HBP1 WT and

CKO mice collected on days 1 and 2 after the cerulein treatment using the 10x Genomics Visium system (Fig. 4A, n=3 each group, see methods). We obtained the median number of genes per spot between 500 and 5000 and the median number of UMI counts per spot between 2000 and 10000 (Fig. S4A). After removing lymph node tissues, we integrated transcriptomes from all samples using Harmony[42] to reduce the technical variations among tissue sections (Fig. 4A). The cell cycle did not affect the distribution of transcriptomes among samples, and the Spearman correlation coefficient among samples was above 0.9, ensuring further analysis (Fig. S4B-C).

We clustered spatial spots into eight groups based on their spatial relationships and gene expression patterns within the tissue using the Louvain algorithm (Fig. 5A, S4D), with different groups representing distinct cell types. Group 0: macrophage; Groups 1 and 2: pancreatic exocrine cells; Group 3: myofibroblast and myeloid cells; Group 6: pancreatic islet cells; Group 7: Collagen expressing fibroblast cells (Fig. 4B-E, S4E-G). Although cells from HBP1 WT and CKO pancreata were distributed across all clusters, those from CKO pancreata were slightly enriched in groups 0, 3, and 7, reflecting the severity of pancreatitis in CKO mice (Fig. S4H). The expression of genes encoding proinflammatory cytokines crucial for recruiting monocytes in HBP1 CKO mice (e.g., MCP1/CCL2, IL6, IL18, ILβ, TNFα) was higher in cells from CKO pancreata, supporting that HBP1 ablation increased macrophage infiltration by regulating proinflammatory cytokine genes (Fig. 4F). Regenerating Gene (Reg) family proteins are crucial protective factors associated with pancreatitis to aid the recovery of pancreatic acinar cells by exerting anti-apoptotic and anti-inflammatory effects in response to oxidative stress in pancreatitis[45, 46]. Indeed, the expression of Reg genes was significantly lower in HBP1 CKO compared to WT pancreata post-cerulein treatment (Fig. S4I-M), confirming that the spatial transcripts reflected the pathophysiological events.

To understand gene programs impacted by HBP1 CKO in the pancreata, we characterized differentially regulated genes (DEG) between HBP1 WT and CKO pancreata in group 2 cells, which are mainly pancreatic acinar cells (Fig. 4A-B). Consistent with the main function of HBP1

as a transcriptional repressor, most DEG were upregulated in HBP1 CKO pancreata (Fig. 4G). Programs related to the immune response were significantly increased in HBP1 CKO pancreatic group 2 cells (Fig. 4H). In contrast, genes encoding digestive enzymes, such as lipases (Pnliprp2 and Pnlip) and SPINK1/SPINK3 protease inhibitors, and molecules related to anti-inflammation (Reg3d, Tff2) and metabolism (Ggh, Nucb2) were among a small number of genes downregulated in CKO pancreata, indicating that HBP1 ablation reduced pancreatic protection against injury (need to incorporate figure).

To gain insight into the effect of HBP1 ablation in the entire pancreata, we analyzed DEG in HBP1 CKO compared to WT pancreata across all cell groups (Fig. 4I-J). Reflecting the severity of pancreatitis, pancreatic acinar genes and Spink1 were significantly downregulated in HBP1 CKO compared to WT pancreata, as expected (Fig.4I and S4N).

Gene ontology (GO) of DEG indicated that, compared to WT pancreata, intracellular transport and cytokine response were significantly increased whereas pathways associated with response to stress, including oxidative stress, were significantly decreased in HBP1 CKO pancreata (Fig. 4J-L). Events such as apoptosis, senescence, and autophagy occur in response to oxidative stress[47-50]. HBP1 is known to increase senescence[22-24]. Apoptotic gene programs were decreased in both HBP1 WT and KO pancreata at 48h after cerulein treatment (S4P-Q) and apoptotic cells were minimally impacted by HBP1 ablation (Fig. 5A-D). Interestingly, ablation of HBP1 significantly downregulated genes involved in autophagy flux, including p21 and p62 involved in autophagosome formation, Chmp4b and Clu involved in autophagosome fusion with lysosomes, and cd63 involved in degradation (Fig. 4M, S4T-V).

In sum, defective anti-oxidative stress in HBP1 CKO pancreata increases acinar necrosis and Reg proteins while increasing the immune response.

Loss of HBP1 in AP impairs autophagy flux directly regulated by HBP1. To determine whether impaired autophagy gene programs resulted in the accumulation of autophagosomes,

we investigated p62 and LC3-II proteins in HBP1 CKO and WT pancreata after cerulein treatment. Cell punctates containing LC3 and p62 increased in HBP1 CKO compared to WT pancreata, indicating delayed clearance of autophagosomes in HBP1 CKO (Fig. 5E-L).

To verify whether HBP1 activation was sufficient to regulate the autophagy gene program at the transcriptional level, we created inducible HBP1-expressing human normal pancreatic ductal epithelial cells (PDEC). We performed RNA-seq 24 hr after HBP1 induction (Fig. S5A-D) and found that, as expected, overexpressing HBP1 downregulated Cyclin D genes (Fig. S5E) and upregulated p21 and BAD genes (Fig. S5F). Upregulation of HBP1 also significantly increased autophagy gene programs (Fig. S5G), including TF genes crucial for autophagosome formation, autophagosome-lysosome fusion and autophagosome degradation, such as FOXO1, FOXO3, and TFEB, and key genes in the autophagy pathways (Fig. S5I-M). Altogether, we demonstrated that HBP1 expression could change the overall autophagy flux gene program.

In sum, these findings suggest that impaired cellular protective mechanisms in HBP1 CKO pancreata contribute, at least in part, to severe pancreatitis driven by impaired autophagy.

Ablation of HBP1 delays the onset of oncogenic KRAS-driven PanIN formation and PanIN progression. We then sought to determine whether HBP1 impacted the onset and progression of PanINs. Thus, we generated p48^{Cre}; LSL-Kras^{G12D}; Hbp1$^{flox/flox}$ mice (Hbp1-null or homozygous KCH), which allow both activating an oncogenic Kras and deleting Hbp1 in pancreatic epithelial cells (Fig. 6A). As an HBP1 WT control, littermate Hbp1 heterozygous mice (Hbp1-competent or heterozygous KCH) were used. Both homozygous and heterozygous KCH mice were born at the expected frequency. Mouse body weight and normalized pancreatic weight did not differ between sexes or among genotypes (Fig. S7A-B).

KC mice showed the full spectrum, albeit slow, progression of PDAC from predominantly PanINs at 4-5 months to rare invasive PDAC and metastatic disease by 10 months[51]. Histological analysis showed that KC mice harbored predominantly focal low-grade PanINs with abundant

intact normal acinar compartments by 20 weeks (Fig. Sx). By ten weeks, HBP1-competent KCH mice developed strong inflammation with a mixture of PanINs in over half of the acinar pancreatic parenchyma, whereas HBP1 null KCH mice showed delayed PanINs formation (Fig. 6B-D). With age, most of the acinar pancreatic parenchyma was significantly replaced by an intense stroma reaction with diffused PanINs (Fig. 6B-F, $p<0.05$). Pancreatic neoplastic lesions, including PanINs, can derived from either acinar cells through metaplasia or spontaneously from pre-existing ductal cells[52-54]. Both metaplasia and spontaneous PanINs were seen in KCH mice (Fig. 6G-H).

By 40 weeks, both HBP1 competent and null pancreata exhibited a subset of lesions with cytological atypia, such as luminal necrosis, cribriform, and budding off of small clusters of epithelial cells into the lumen, seen in high-grade PanINs (Fig. 6I-J). However, the overall nuclear abnormalities increased with age only in HBP1-competent, but not in HBP1-null, KCH mice (Fig. 6I-J). The majority of PanINs in HBP1-null mice were well-differentiated low-grade PanIN1-like, including non-invasive large cystic tumors (Fig. S7-need to add). Consistently, the ratio of proliferating cells from Alcian Blue positive PanINs was significantly lower in HBP1-null mice than in HBP1 competent mice at 40 weeks, indicating that HBP1-null mice predominantly formed less aggressive PanIN (Fig. 6K).

In summary, HBP1 ablation in KC mice delays the initiation of KrasG12D-driven PanIN formation, limits nuclear atypia, and restricts PanIN progression, potentially through mechanisms involving autophagy.

Discussion.

In order to better predict and target the pathological progression of AP, a deeper understanding of molecular regulators of the AP progression is needed. Here, we show that increased HBP1 expression coincides with pancreatitis and is associated with pancreatitis progression and that HBP1 ablation exacerbates acinar inflammatory damage through necrosis and autophagy dysregulation. We further show that, in the presence of an oncogenic Kras, HBP1 ablation

accelerates PanIN formation but impairs PanIN progression to higher grades. These results suggest that HBP1 is crucial in preventing pancreatitis and in supporting PanIN progression by maintaining cellular homeostasis.

Necrotizing pancreatitis, which has a worse prognosis than interstitial edematous pancreatitis, is marked by increased acinar cell loss[5, 7, 8]. Disrupting acinar homeostasis and impaired autophagy can exacerbate pancreatitis by cell death[9-11]. Our data show that HBP1 ablation leads to acinar dropout due to necrosis, not apoptosis, and that dysregulated autophagy is increased in HBP1 CKO compared to HBP1 WT pancreata. Our data further show that HBP1 ablation decreases whereas its overexpression increases the expression of key autophagy regulators and that HBP1 overexpression also increases LAMP3 and TFEB, proteins in conjugating autophagosomes with lysosomes. These data, therefore, indicate that HBP1 may regulate both autophagosome formation and autophagosome conjunction with lysosomes. Thus, HBP1 may serve as a gatekeeper against acinar necrosis and disease progression, at least in part, by regulating the autophagy flux. How HBP1 regulates the expression of these factors and impacts the overall autophagy flux remains to be determined.

Dysregulated autophagy and acinar cell death in HBP1 CKO mice likely would enhance inflammation. Macrophage recruitment is a key factor affecting the pancreatitis severity[55, 56]. Indeed, HBP1 ablation in pancreata broadly increases cells in pancreata expressing TNF-α, NF-κB, IL-6, IL-18, and MCP2, which are proinflammatory cytokines crucial for monocyte infiltration. Moreover, the expression of Reg family members (Reg3a, Reg3b, and Reg3d) is significantly downregulated in HBP1 CKO mice after cerulein treatment. Indeed, Reg family members, whose expression is typically upregulated during pancreatitis, modulate the immune response to protect against pancreatic damage, while their downregulation aggravates inflammation[46, 57, 58].

Interestingly, in the presence of an oncogenic Kras, HBP1 ablation delays the onset of PanIN formation and limits PanIN progression. Given that autophagy is essential for PanIN and PDAC growth, we speculate that HBP1 plays a critical role in regulating autophagy during PanIN

progression. Further studies will be necessary to investigate whether HBP1 ablation prevents PanIN progression without tumor suppressors.

In conclusion, HBP1 neo-expression limits inflammatory injury by maintaining acinar homeostasis and reducing macrophage infiltration. In the presence of an oncogenic KRAS mutant, neo-accumulation of HBP1 is required for PanIN progression. Targeting both HBP1 and autophagy offers a potential dual therapeutic approach: enhancing autophagy in pancreatitis to resolve inflammation while inhibiting autophagy in PanINs to prevent tumor progression. This strategy could effectively manage both conditions.

ACKNOWLEDGMENTS

We thank Drs. Cote and Zimmers for comments on the manuscript; Drs. Ohtsuka and Kitano (Kyoto) and Fedorov (OHSU Transgenic Mouse Models) for fertilized the embryos of Hbp1$^{floxed/floxed}$ strain and generating p48^{Cre}; HBP1$^{floxed/floxed}$ mice, respectively; K. Rice, M. Davenport, and Y. Wang for their technical assistance; OHSU Shared Resource (Histopathology, Transgenic Mouse Models); Brenden-Colson Center for Pancreatic Care and the Oregon Pancreas Tissue Registry (IRB #3609).

MAIN FIGURE/TABLE TITLES and LEGENDS

Figure 1. The expression of HBP1 shifts from pancreatic islets to acinar cells in pancreatitis.

A. Schematic diagram of cerulean-induced AP model. B-E. Representative images of HBP1 immunostaining in the pancreata of one set of mice on day 0 (B, inset b'), 1 (C, inset c'), 2 (D, inset d'), and 7 (E, inset e'). n=3 each time point, images from the rest of mice are shown in Figure S1. F-K. Representative H&E images (F, H, J) and immunofluorescent images of HBP1 expression (G, I, K) on normal-looking acinar (F, G), injured acinar cells (H, I), and PanINs cells (J, K) from patients with pancreatitis. Scale bars represent 100 μm (top images) or 10 μm (bottom images). L. Summary of HBP1 levels among human pancreatic tissues (270 tissues from 49 patients with pancreatitis and 16 normal other tissues). The expression level of HBP1 in injured acinar cells or PanINs is significantly higher than in normal controls. (*** indicates $p<0.000001$, unpaired Welch t-test). M-O. ROC curves and AUC values of HBP1 expression for each cell type (M, O) and for the combined cell types (N, O) in pancreatitis patient tissues, which were analyzed against the presence of pancreatitis with cancer.

Figure 2. Hbp1 ablation exaggerates acute pancreatitis phenotype in the cerulean-induced AP model. A. Diagram of cerulein-induced AP model. Cerulein was injected every hour for seven injections. Mice were sacrificed 1, 2, and 7 days after the last injection and their pancreata were investigated. B-C. Body weight (B) and pancreatic weight normalized with body weight (C) of mice of indicated sexes at each time point. There is no significant difference in body weight between female and male mice (B). Compared to PBS controls, normalized pancreatic weight is significantly higher in Cerulein-treated both HBP1 WT (p-values are labeled in blue) and HBP1 CKO (p-values are labeled in red) mice in day 1 and in only HBP1 WT mice (blue) in day 2. P-values significantly different between WT and CKO are labeled with purple. The unadjusted p-

values are calculated based on the two-sample t-test without the equal variance assumption. Linear models include group indicators and sex indicators as covariates that are fitted to the outcome of interest (weight, pan weight, or norm pan weight). The p-values corresponding to the coefficient of the group indicator are reported as the adjusted p-values. D. Binary scoring table of the presence of pancreatitis. The presence of pancreatitis was determined by the pathologist based on H&E images in an unblinded manner. E. Representative H&E images of pancreatitis in HBP1 WT control and HBP1 CKO mice. Scale bars indicate 50 μm. F. Pancreatitis severity scoring table, based on H&E images. G. The severity of pancreatitis in HBP1 WT control and CKO mice was determined on days 1, 2, and 7 after cerulein induction. Statistical analysis was made using two-part fitted models (p=0.01 for 24hr, p=0.03 for 48 hrs, n=10-12 per group at each time point).

Figure 3. Loss of HBP1 increases myofibroblasts and myeloid lineage cells in AP. A. Schematic diagram of DSP. A total of 24 pancreatitis cores from two mice per group and time point were applied for the DSP mouse immune cell profiling core, including immune activation status, immune cell typing and immune-oncology drug target protein modules[39]. B. Clustering analysis. Blue brackets indicate the pancreata from HBP1 WT mice and red brackets indicate the pancreas from HBP1 CKO mice. C. The expression of marker proteins for proliferation (Ki67), metabolism (GAPDH), and of Pan-CK proteins. D-E. Significantly increased immune cell markers in HBP1 CKO mice compared to WT mice on day 1 (D) and 2 (E) post-Cerulein. F. Representative images of immunostaining for F4/80^{+} macrophages and CD4^{+} cells in the pancreatic parenchyma during injury induced by cerulein treatment (n=3).

Figure 4. Hbp1 ablation impairs cellular response to oxidative stress in the cerulean-induced acute AP model.

A. Schematic diagram of Visium Spatial transcriptomic analysis of pancreata derived from HBP1 WT and CKO mice 24h and 48hrs after cerulein treatments (n=3, each type). Transcriptomics obtained from each sample are integrated to reduce variations among tissue sections. B. Uniform Manifold Approximation and Projection (UMAP) displayed eight clusters of integrated samples. C-E. The expression of pancreatic acinar (C), islet cells (D), and macrophage (E) marker genes. The X-axis indicates each cluster. The Y-axis indicates log2 transformed normalized UMI counts per spot. F. Mapping of proinflammatory genes in the UMAP. HBP1 WT or CKO pancreata are displayed in UMI. Each dot represents each spot expressing cytokine genes, displayed in log2-normalized UMI counts. G-H. Heatmap (G) and Top 5 GO terms (H) of differentially expressed genes in group 2 cells between CKO and WT at day 1. I. the expression of the Spink1 gene. J-K. Top 5 GO terms of genes differentially upregulated (J) and downregulated (K) in HBP1 CKO compared to WT mice in both time points. L. Genes in the cellular response to oxidative stress. M. The expression of genes in senescence and autophagy pathways among DEG.

Figure 5. Representative images of immune staining for cleaved caspase-3 (A-D, arrow; positive signals) and IF for autophagosome marker proteins LC3 (E-H) and p62 (I-L) in pancreata from HBP1 WT and CKO mice on day 1 and day 2 after cerulein treatment (replicates n=3).

Figure 6. PanIN progression is delayed in HBP1 null mice (KCH-homozygous) compared to HBP1 competent mice (KCH-heterozygous). A. Diagram and representative image of KCH mice. B-C. The fraction of pancreatic parenchyma representing acinar (B) and PanINs (C). Normal acinar cells significantly decreased with age in both groups (B). The fraction of PanINs is significantly lower in KCH null mice compared to KCH competent mice at 10 weeks but significantly increases from 20 to 40 weeks in KCH null mice (Welch t-test). D-F. The fraction of total ducts representing each PanIN stage at 10 weeks (D), 20 weeks (E), and 40 weeks (F) of

KCH-competent and null mice. The fraction of ducts representing PanIN1 and PanIN2 significantly differed between these two genotypes by 20 weeks and 40 weeks, respectively. (Welch t-test, KCH-null (n=8), KCH-competent (n=5)). G-J. Representative H&E images of KCH mice. By 10 weeks of age, HBP1-null mice generate PanIN-like cells from acinar origins (G, inset g') and spontaneously from ductal cells (H, inset h'). By 40 weeks, both HBP1-competent and HBP1-null mice develop cytological high-grade PanINs (I-J). HBP1-competent mice form high-grade PanINs with nuclear atypia (I, inset i', i-i, i-ii) whereas HBP1-null mice form PanINs with non-nuclear atypia (J, inset j', j-i, j-ii, arrow: luminal necrosis). K. The ratio of Ki67 expressing cells over Alcian blue positive PanINs per mm^2 at 40 weeks. (six random regions of each mouse are measured, 6 for HBP1-heterozygotic n=6, homozygotic mice =11 Welch t-test).

Supplementary figure legends

Figure S1. Pancreatic HBP1 accumulation gradually decreases throughout tissue regeneration. Related to Figure 1. A-B. Validation of HBP1 antibody specificity by peptide competition assay. A rabbit polyclonal anti-HBP1 antibody was incubated with no competitor (A) or with a 100-fold molar excess of recombinant HBP1 peptide (B) for 30 min at room temperature and then applied to the immune staining. The excess HBP1 competes for the signal. C-I. Expression of HBP1 during Cerulein-treated pancreatitis. Images from no primary antibody control (C) and two additional mice are shown in D-I. (J-K) The fitted logistic regression model for combined cell types (J) and each cell type (K).

Figure S2. Generation of pancreatic Hbp1 CKO mice. Relevant to Figure 2. A. A schematic diagram of a part of the Hbp1 locus (chr12:31920507-31956193) of $Hbp1^{flox/flox}$ mice. One loxP site is integrated into the intron 1 and another loxP and Frt sites are integrated into the intron 2. After crossing with $p48^{Cre}$ mice, Cre recombinase deletes the DNA between the two loxP sites in $Hbp1^{flox/flox}$ mice and generates $p48^{Cre}$; $Hbp1^{flox/WT}$. To make homozygotic $p48^{Cre}$; $Hbp1^{flox/flox}$, the heterozygous mice are repetitively bred with each other. B. Representative agarose gel images to verify the insertion of loxP and loxP/FRT sites in intron 1 and intron 2, respectively. Using Hbp1 loxP site primers in intron1, Hbp1 WT and floxed alleles give rise to 173 bp and 219 bp, respectively. Using Hbp1loxP FRT site primers in intron 2, Hbp1 WT and floxed alleles produce 184 bp and 272 bp, respectively. C. Confirmation of missing the part of Hbp1 mRNA encoded by the exon 2 using real-time PCR. Real-time PCR primers are designed to detect parts of the Hbp1 mRNAs encoded by exon1/2, exon6/7, and exon 10-11. Duodenum and pancreatic tissues from control mice with the intact HBP1 alleles are used as negative and positive controls, respectively. The Y-axis shows Hbp1 mRNA levels relative to gapdh. The pancreata from CKO mice lacking Hbp1 alleles show the complete absence of Hbp1 exon1/2 mRNAs, which is a level relatively similar to negative controls, compared to control mice with intact Hbp1 alleles (* $p<0.005$, Welch

t-test, n=6 technical replicates). D-I. Confirmation of the absence of HBP1 protein in HBP1 CKO mice. Representative H&E (D, G), HBP1 IHC (E-F, H-I) on pancreatic islet cells from control and CKO mice. J. Amylase and CK19 staining on pancreata from HBP1 WT control (upper) and HBP1 CKO (lower) mice on day 0, 1, 2, 7 after cerulein treatment.

Figure S3. Relevant to Figure 3. A. Volcano plots of proteins with geomean normalized counts. The X-axis indicates log 2-fold differences between CKO and WT pancreata and the Y-axis indicates -log 10 (p-value). We selected proteins that significantly increased (Red) or decreased (Blue) over 1.5-fold in CKO compared to WT ($p<0.01$). Non-significantly regulated proteins are in gray. Raw N-count was normalized with signal-to-noise ratio (SNR). Significantly regulated proteins are defined based on p-value and fold changes (FC: HBP1 CKO/WT). P-values are less than 0.01, and the expression ratio of markers in CKO over WT is larger than 1.5-fold. Log2 (FC)>0.585. B-C. Top proteins downregulated in HBP1 CKO pancreata 24h (B) and 48h (C) post-Cerulein treatment. D. The representative images of F4/80$^+$ and CD4$^+$ T cells in the peripancreatic lymphoid node tissues during injury after cerulein treatment.

Figure S4. Relevant to Figure 5. A. Scatter plot of median gene numbers and median UMI counts at 20K reads in each spot. B. UMAP of cell cycle genes. C. Spearman correlation coefficient among samples. D. UMAPI of eight clusters in each group. E-G. Network analysis of top DEG in group 2 (E), group 6 (F), and group 3 (G). H. UMAP of aggregated clusters in each group. I-M. Expressions of the Reg family genes Reg2 (I), Reg3a (J), Reg3d (K), Reg3b (L) and Reg3g (M). N. Expression of acinar genes. O. KRT19 expression. P. GO terms of genes that are increased in day 1 compared to day 2. Q. The expression of apoptotic pathway genes. R. Expression of Foxo3. S. Go terms of genes enriched on day 2. T-V. Expression of autophagy genes.

Figure S5. Relevant to Figure 5. Confirmation of autophagy gene program regulated by HBP1 in human normal pancreatic ductal epithelial cells (PDEC). A. Diagram of inducible human HBP1 (iHBP1) overexpressing (OE) lentiviral vector for generating inducible HBP1 expressing PDEC. B. Schematic flowchart of RNA-seq from iHBP1-PDEC, C. Validation of iHBP1-PDEC. D-F. Validation of doxycycline-dependent expression of HBP1 (D) and HBP1-regulated cyclin D genes (E) and p21 and BAD (F). The X-axis indicates concentrations of doxycycline (0, 0.1, 1 μg/ml), and the Y-axis indicates normalized DESEQ2 counts. G. Top5 GO of DEG upon HBP1 expression in iHBP1 OE PDEC (FDR<0.05). Blue bars indicate the number of genes expected to enrich, and red bars indicate the number of genes that are actually enriched. H-M. Expression of genes in autophagy pathways among DEG. The direct master TFs (H) and key genes for autophagosome initiation, formation, and expansion (I-J), autophagosome-lysosome fusion (K-L), and the degradation of autophagosome-lysosomal (M).

Figure S6. Relevant to Figure 5. Additional immune staining of LC3 (A-D) and p62 (E-H) autophagosome marker proteins in pancreata from HBP1 WT and CKO mice on day 1 and day 2 after cerulein treatment.

Figure S7. Relevant to Figure 6 KCH mice. A-B. Body weight (A) and pancreatic weight normalized by body weight (B) in each sex for KC and KCH mice. There was no difference between sex. C-E. The fraction of normal acinar (C), PanINs (D), and ducts representing each PanIN in 20 and 40 weeks (E) in KC mice. F-G. The comparison of fraction of acinar (F) and PanINs (G) over time among KC, KCH- heterozygous and homozygous mice.

REFERENCES

1. Mederos MA, Reber HA, Girgis MD. Acute Pancreatitis: A Review. JAMA 2021;325:382-390.
2. Forsmark CE, Vege SS, Wilcox CM. Acute Pancreatitis. N Engl J Med 2016;375:1972-1981.
3. Lee PJ, Papachristou GI. New insights into acute pancreatitis. Nat Rev Gastroenterol Hepatol 2019;16:479-496.
4. Greer JB, Whitcomb DC. Inflammation and pancreatic cancer: an evidence-based review. Curr Opin Pharmacol 2009;9:411-8.
5. Banks PA, Bollen TL, Dervenis C, et al. Classification of acute pancreatitis--2012: revision of the Atlanta classification and definitions by international consensus. Gut 2013;62:102-11.
6. Wiley MB, Mehrotra K, Bauer J, et al. Acute Pancreatitis: Current Clinical Approaches, Molecular Pathophysiology, and Potential Therapeutics. Pancreas 2023;52.
7. Eisses JF, Davis AW, Tosun AB, et al. A computer-based automated algorithm for assessing acinar cell loss after experimental pancreatitis. PLoS One 2014;9:e110220.
8. Leppäniemi A, Tolonen M, Tarasconi A, et al. 2019 WSES guidelines for the management of severe acute pancreatitis. World Journal of Emergency Surgery 2019;14:27.
9. Gukovskaya AS, Gukovsky I, Algul H, et al. Autophagy, Inflammation, and Immune Dysfunction in the Pathogenesis of Pancreatitis. Gastroenterology 2017;153:1212-1226.
10. Antonucci L, Fagman JB, Kim JY, et al. Basal autophagy maintains pancreatic acinar cell homeostasis and protein synthesis and prevents ER stress. Proc Natl Acad Sci U S A 2015;112:E6166-74.
11. Xia L, Xu Z, Zhou X, et al. Impaired autophagy increases susceptibility to endotoxin-induced chronic pancreatitis. Cell Death & Disease 2020;11:889.
12. Hofbauer B, Saluja AK, Lerch MM, et al. Intra-acinar cell activation of trypsinogen during caerulein-induced pancreatitis in rats. Am J Physiol 1998;275:G352-62.
13. Halangk W, Lerch MM, Brandt-Nedelev B, et al. Role of cathepsin B in intracellular trypsinogen activation and the onset of acute pancreatitis. J Clin Invest 2000;106:773-81.
14. Murtaugh LC, Keefe MD. Regeneration and repair of the exocrine pancreas. Annu Rev Physiol 2015;77:229-49.
15. Lugea A, Nan L, French SW, et al. Pancreas recovery following cerulein-induced pancreatitis is impaired in plasminogen-deficient mice. Gastroenterology 2006;131:885-99.
16. Krah NM, De La OJ, Swift GH, et al. The acinar differentiation determinant PTF1A inhibits initiation of pancreatic ductal adenocarcinoma. Elife 2015;4.
17. Morris JPt, Cano DA, Sekine S, et al. Beta-catenin blocks Kras-dependent reprogramming of acini into pancreatic cancer precursor lesions in mice. J Clin Invest 2010;120:508-20.
18. Lesage F, Hugnot JP, Amri EZ, et al. Expression cloning in K+ transport defective yeast and distribution of HBP1, a new putative HMG transcriptional regulator. Nucleic Acids Res 1994;22:3685-8.
19. Lavender P, Vandel L, Bannister AJ, et al. The HMG-box transcription factor HBP1 is targeted by the pocket proteins and E1A. Oncogene 1997;14:2721-8.
20. Tevosian SG, Shih HH, Mendelson KG, et al. HBP1: a HMG box transcriptional repressor that is targeted by the retinoblastoma family. Genes Dev 1997;11:383-96.
21. Shih HH, Tevosian SG, Yee AS. Regulation of differentiation by HBP1, a target of the retinoblastoma protein. Mol Cell Biol 1998;18:4732-43.
22. Zhang X, Kim J, Ruthazer R, et al. The HBP1 transcriptional repressor participates in RAS-induced premature senescence. Mol Cell Biol 2006;26:8252-66.
23. Wang S, Cao Z, Xue J, et al. A positive feedback loop between Pim-1 kinase and HBP1 transcription factor contributes to hydrogen peroxide-induced premature senescence and apoptosis. J Biol Chem 2017;292:8207-8222.
24. Li H, Wang W, Liu X, et al. Transcriptional factor HBP1 targets P16(INK4A), upregulating its expression and consequently is involved in Ras-induced premature senescence. Oncogene 2010;29:5083-94.
25. Yang R, Zhou Y, Zhang T, et al. The transcription factor HBP1 promotes ferroptosis in tumor cells by regulating the UHRF1-CDO1 axis. PLoS Biol 2023;21:e3001862.
26. Cao Z, Xue J, Cheng Y, et al. MDM2 promotes genome instability by ubiquitinating the transcription factor HBP1. Oncogene 2019;38:4835-4855.
27. He S, Yang S, Niu M, et al. HMG-box transcription factor 1: a positive regulator of the G1/S transition through the Cyclin-CDK-CDKI molecular network in nasopharyngeal carcinoma. Cell Death Dis 2018;9:100.

28. Sanghvi VR, Mavrakis KJ, Van der Meulen J, et al. Characterization of a set of tumor suppressor microRNAs in T cell acute lymphoblastic leukemia. Sci Signal 2014;7:ra111.
29. Bollaert E, Johanns M, Herinckx G, et al. HBP1 phosphorylation by AKT regulates its transcriptional activity and glioblastoma cell proliferation. Cell Signal 2018;44:158-170.
30. Xiu M, Kim J, Sampson E, et al. The transcriptional repressor HBP1 is a target of the p38 mitogen-activated protein kinase pathway in cell cycle regulation. Mol Cell Biol 2003;23:8890-901.
31. Mohamed WI, Park SL, Rabl J, et al. The human GID complex engages two independent modules for substrate recruitment. EMBO Rep 2021;22:e52981.
32. Lampert F, Stafa D, Goga A, et al. The multi-subunit GID/CTLH E3 ubiquitin ligase promotes cell proliferation and targets the transcription factor Hbp1 for degradation. Elife 2018;7.
33. Kim J, Ekstrom T, Yang W, et al. Longitudinal analysis of human pancreatic adenocarcinoma development reveals transient gene expression signatures. Mol Cancer Res 2021.
34. Nakhai H, Sel S, Favor J, et al. Ptf1a is essential for the differentiation of GABAergic and glycinergic amacrine cells and horizontal cells in the mouse retina. Development 2007;134:1151-60.
35. Jackson EL, Willis N, Mercer K, et al. Analysis of lung tumor initiation and progression using conditional expression of oncogenic K-ras. Genes Dev 2001;15:3243-8.
36. Watanabe N, Kageyama R, Ohtsuka T. Hbp1 regulates the timing of neuronal differentiation during cortical development by controlling cell cycle progression. Development 2015;142:2278-90.
37. Nakao K, Nakagata N, Katsuki M. Production of chimeric mice from cryopreserved blastocysts. Exp Anim 1998;47:167-71.
38. Niederau C, Ferrell LD, Grendell JH. Caerulein-induced acute necrotizing pancreatitis in mice: protective effects of proglumide, benzotript, and secretin. Gastroenterology 1985;88:1192-204.
39. Merritt CR, Ong GT, Church SE, et al. Multiplex digital spatial profiling of proteins and RNA in fixed tissue. Nat Biotechnol 2020;38:586-599.
40. Cui Zhou D, Jayasinghe RG, Chen S, et al. Spatially restricted drivers and transitional cell populations cooperate with the microenvironment in untreated and chemo-resistant pancreatic cancer. Nat Genet 2022;54:1390-1405.
41. Hao Y, Stuart T, Kowalski MH, et al. Dictionary learning for integrative, multimodal and scalable single-cell analysis. Nature Biotechnology 2024;42:293-304.
42. Korsunsky I, Millard N, Fan J, et al. Fast, sensitive and accurate integration of single-cell data with Harmony. Nature Methods 2019;16:1289-1296.
43. Kawaguchi Y, Cooper B, Gannon M, et al. The role of the transcriptional regulator Ptf1a in converting intestinal to pancreatic progenitors. Nat Genet 2002;32:128-34.
44. Calvo EL, Boucher C, Coulombe Z, et al. Pancreatic GAPDH gene expression during ontogeny and acute pancreatitis induced by caerulein. Biochem Biophys Res Commun 1997;235:636-40.
45. Hartupee JC, Zhang H, Bonaldo MF, et al. Isolation and characterization of a cDNA encoding a novel member of the human regenerating protein family: Reg IV. Biochim Biophys Acta 2001;1518:287-93.
46. Hu G, Shen J, Cheng L, et al. Reg4 protects against acinar cell necrosis in experimental pancreatitis. Gut 2011;60:820-8.
47. Filomeni G, De Zio D, Cecconi F. Oxidative stress and autophagy: the clash between damage and metabolic needs. Cell Death Differ 2015;22:377-88.
48. Kannan K, Jain SK. Oxidative stress and apoptosis. Pathophysiology 2000;7:153-163.
49. Navabpour S, Morris K, Allen R, et al. Expression of senescence-enhanced genes in response to oxidative stress. J Exp Bot 2003;54:2285-92.
50. Brandl A, Meyer M, Bechmann V, et al. Oxidative stress induces senescence in human mesenchymal stem cells. Experimental Cell Research 2011;317:1541-1547.
51. Hingorani SR, Petricoin EF, Maitra A, et al. Preinvasive and invasive ductal pancreatic cancer and its early detection in the mouse. Cancer Cell 2003;4:437-50.
52. Hruban RH, Maitra A, Goggins M. Update on pancreatic intraepithelial neoplasia. Int J Clin Exp Pathol 2008;1:306-16.
53. Storz P. Acinar cell plasticity and development of pancreatic ductal adenocarcinoma. Nat Rev Gastroenterol Hepatol 2017;14:296-304.
54. Strobel O, Rosow DE, Rakhlin EY, et al. Pancreatic duct glands are distinct ductal compartments that react to chronic injury and mediate Shh-induced metaplasia. Gastroenterology 2010;138:1166-77.
55. Sendler M, Weiss FU, Golchert J, et al. Cathepsin B-Mediated Activation of Trypsinogen in Endocytosing Macrophages Increases Severity of Pancreatitis in Mice. Gastroenterology 2018;154:704-718 e10.

56. Hu F, Lou N, Jiao J, et al. Macrophages in pancreatitis: Mechanisms and therapeutic potential. Biomedicine & Pharmacotherapy 2020;131:110693.
57. Zenilman ME, Tuchman D, Zheng Q, et al. Comparison of reg I and reg III levels during acute pancreatitis in the rat. Ann Surg 2000;232:646-52.
58. Chen W, Imasaka M, Lee M, et al. Reg family proteins contribute to inflammation and pancreatic stellate cells activation in chronic pancreatitis. Scientific Reports 2023;13:12201.

What You Need to Know

(containing brief summarizations about your study under the following 5 headings: **BACKGROUND AND CONTEXT, NEW FINDINGS, LIMITATIONS, CLINICAL RESEARCH RELEVANCE,** and **BASIC RESEARCH RELEVANCE**. Please provide **25-30** words (about one sentence) under each of the first 3 headings that very briefly and simply summarize your study in relation to each category. The last 2 headings should be no more than **50-60** words (two sentences) each. These should lack abbreviations and have clear language explaining the importance of your results to clinicians and researchers not familiar with your specialty area.)

Background and Context

New Findings

Limitations

Clinical Research Relevance

Basic Research Relevance

LAY SUMMARY (It should be **25-30** words (about one sentence) and very briefly summarize the article's main findings in simple lay terms**)**

Lee & Ekstrom/Kim al.,2024

Figure 1

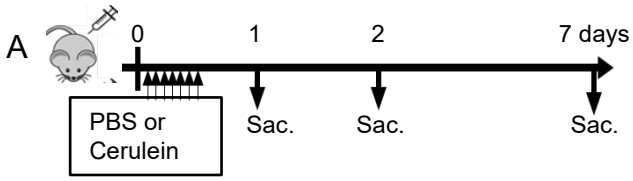

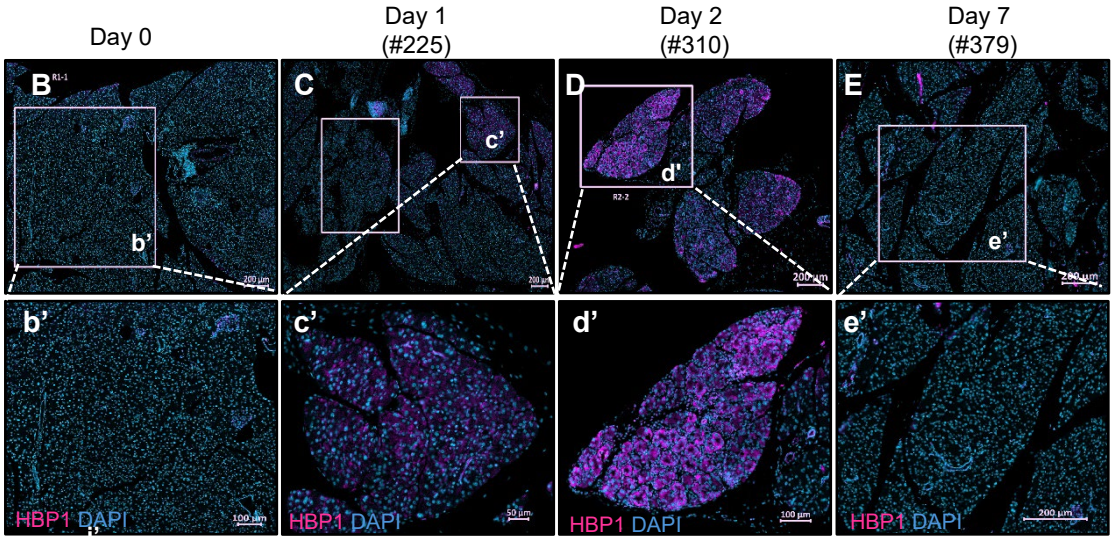

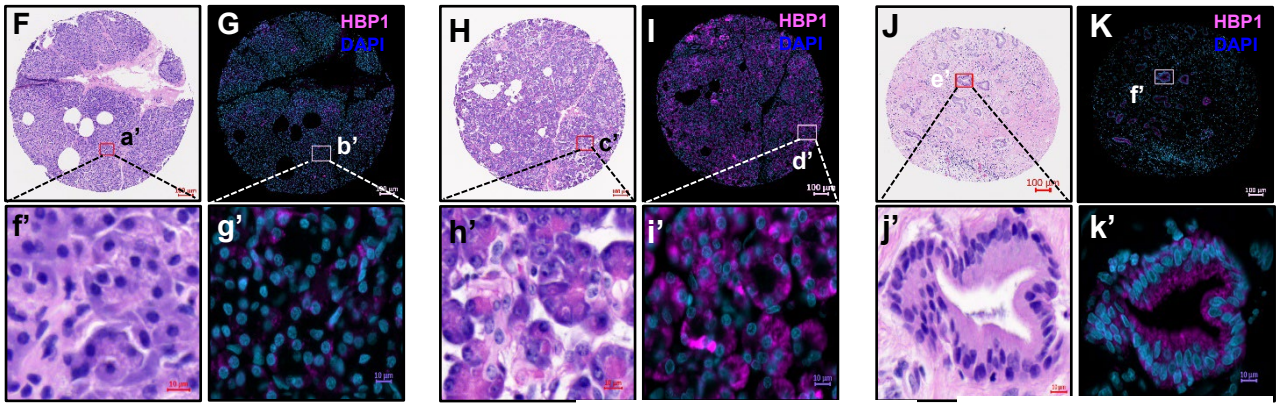

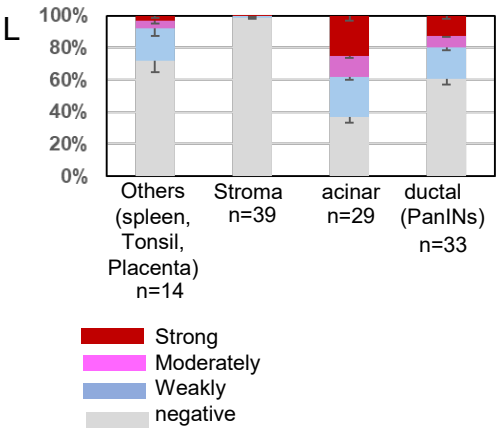

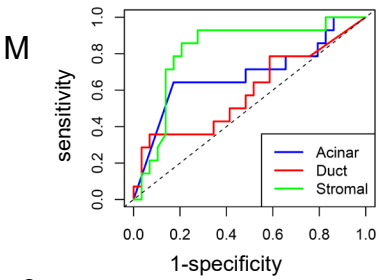

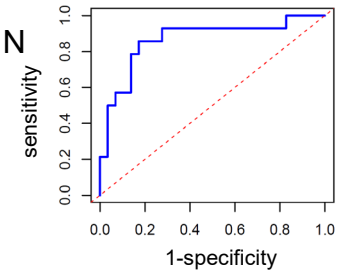

0

Pancreatitis with cancer vs without cancers	unadjusted AUC (95% CI)	age/sex adjusted AUC (95% CI)
acinar	0.69 (0.50-0.87)	0.67 (0.48-0.86)
ductal	0.59 (0.39-0.79)	0.60 (0.41-0.80)
stroma	0.81 (0.68-0.96)	0.84 (0.71-0.98)
combined all three cell types	0.87 (0.74-0.99)	0.88 (0.75-1.00)

Lee & Ekstrom/Kim al.,2024

Figure 2

A

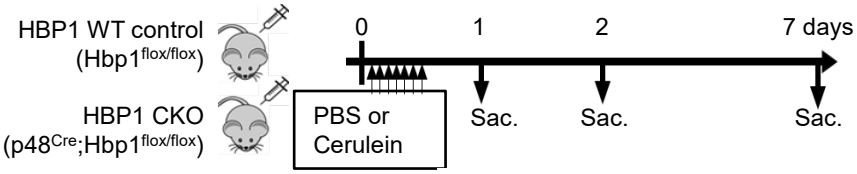

B

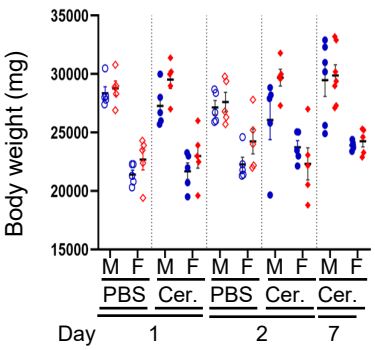

C

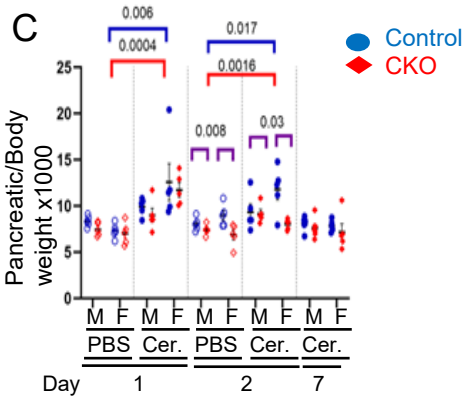

D

		HBP1 WT Control (Hbp1$^{flox/flox}$)		HBP1 CKO (p48^{Cre};Hbp1$^{flox/flox}$)	
		n	pancreatitis positive	n	pancreatitis positive
day 1	total	9	7/9 (78%)	10	10/10 (100%)
	male	5	3/5 (60%)	5	5/5 (100%)
	Female	4	4/4 (100%)	5	5/5 (100%)
day 2	total	10	5/10 (50%)	10	8/10 (80%)
	male	5	4/5 (80%)	5	3/5 (60%)
	Female	5	1/5 (20%)	5	5/5 (100%)
day 7	total	11	0/11 (0%)	12	4/12 (33%)
	male	6	0/6 (0%)	7	2/7 (29%)
	Female	5	0/5 (0%)	5	2/5 (40%)

F

score	severity of inflammation	histology feature
0	absence	normal
1	mild	edema, increased inflammation, no acinar dropout, focal lymphocyte
2	moderate	lymphocyte infiltration & acinar dropout
3	severe	diffused (multifocal), chronic pancreatitis

E

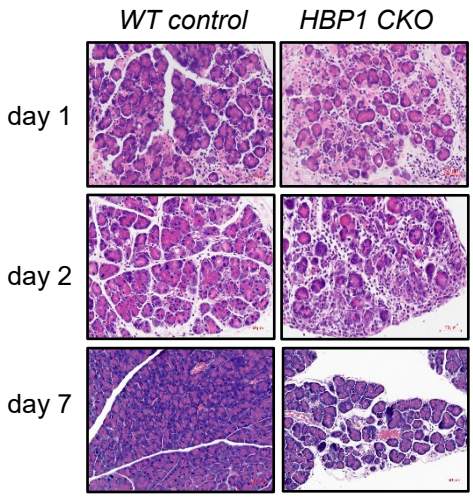

G

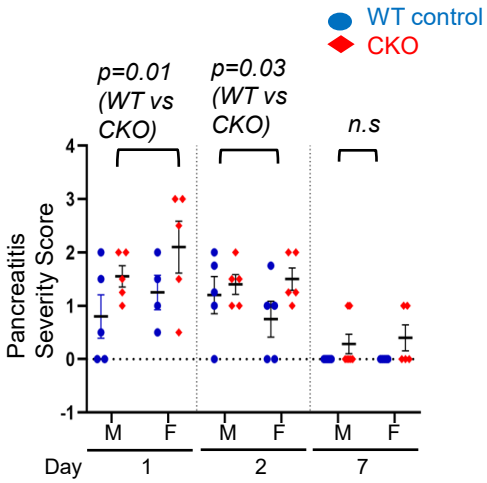

Lee & Ekstrom/Kim al.,2024

Figure 3

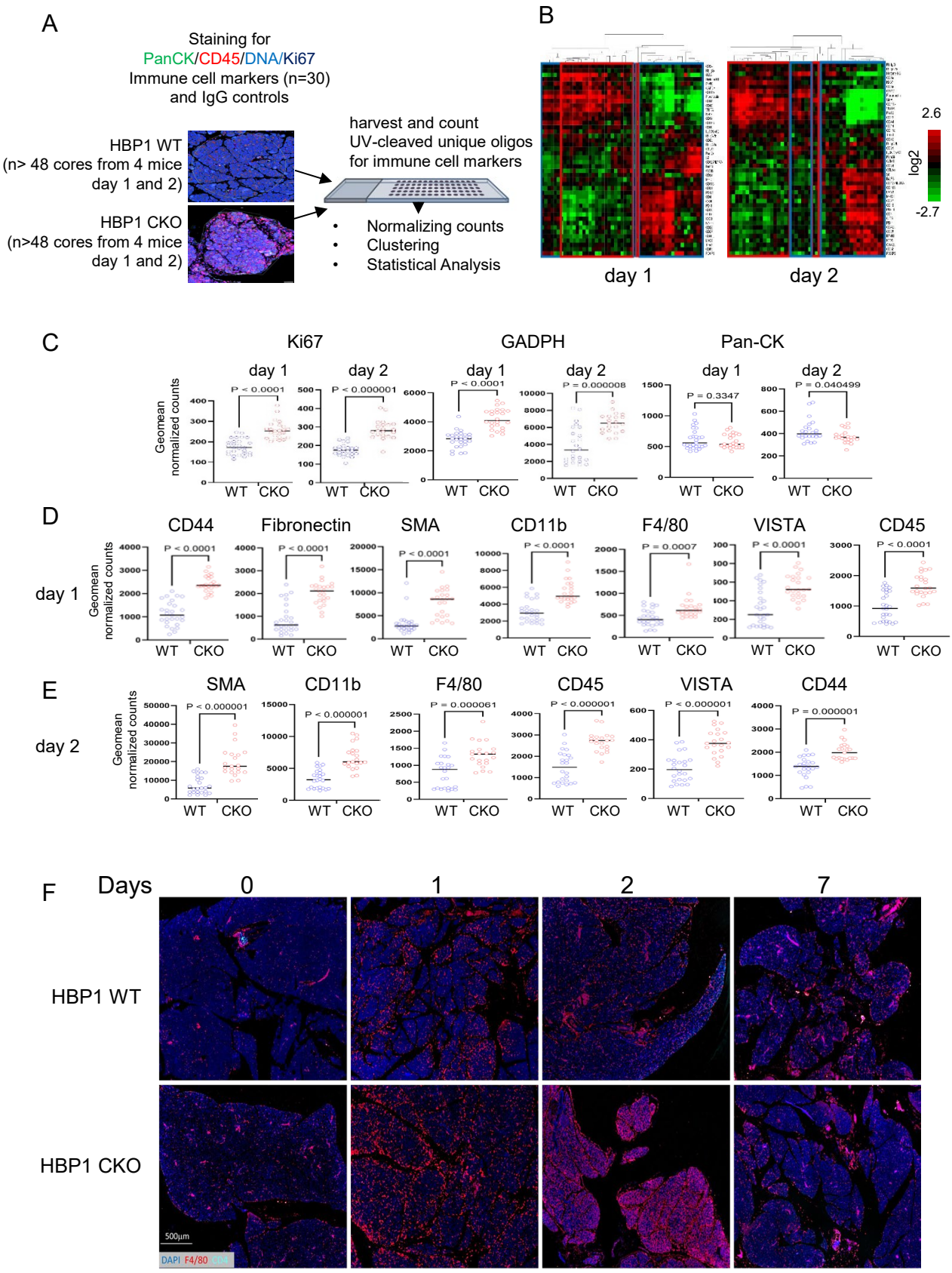

Lee & Ekstrom/Kim al.,2024

Figure 4

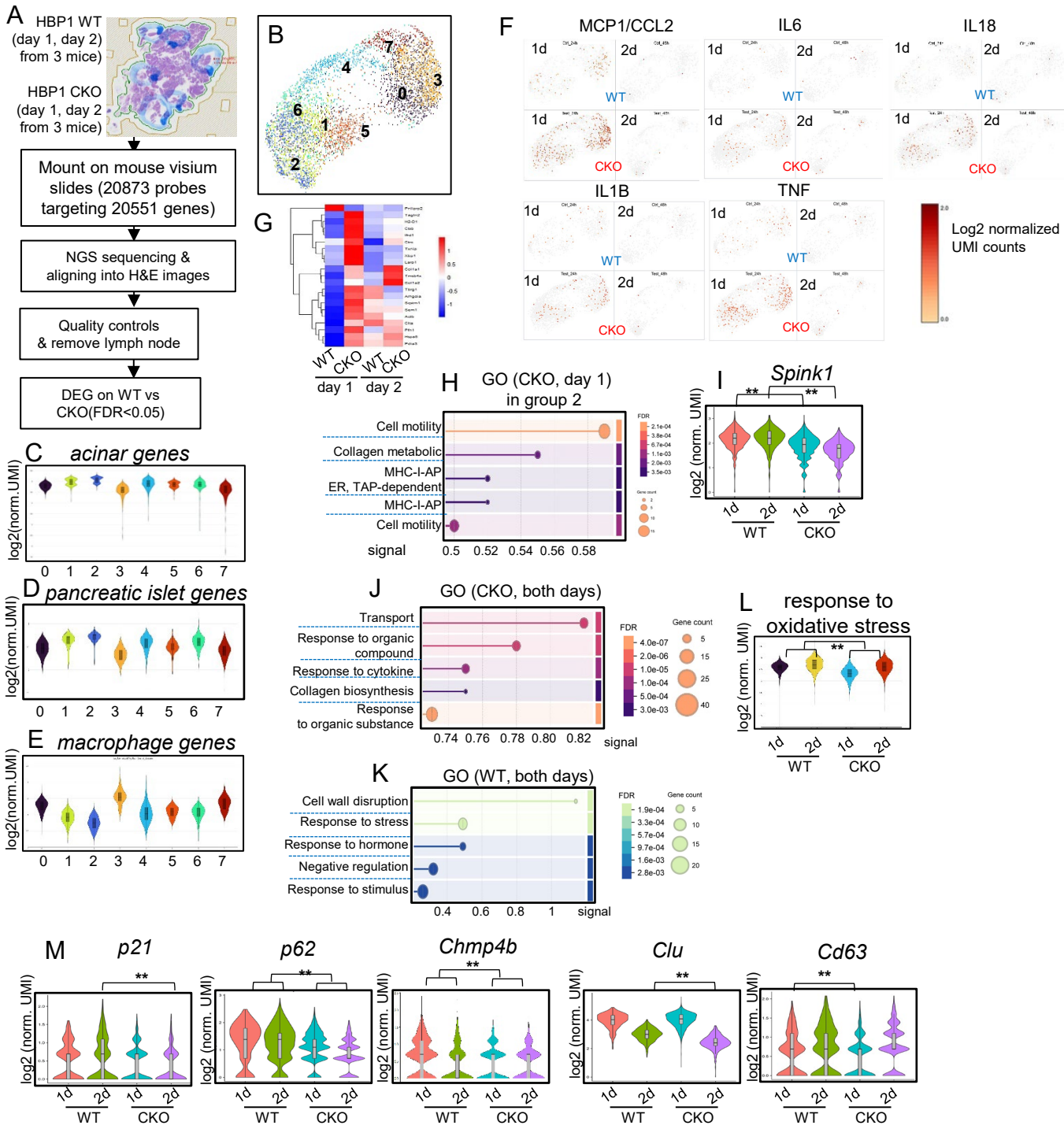

Lee & Ekstrom/Kim al.,2024

Figure 5

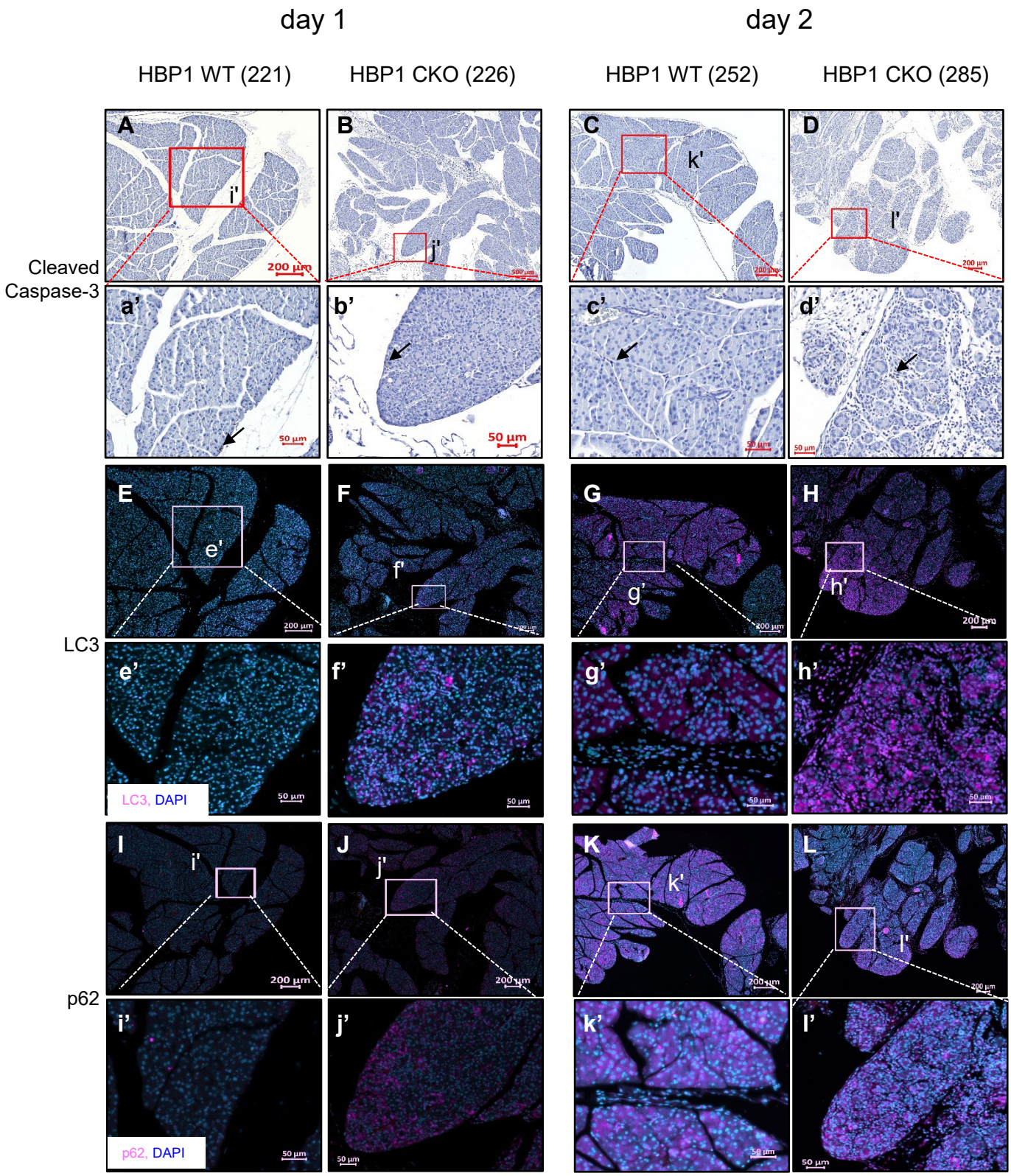

Lee & Ekstrom/Kim al.,2024

Figure 6

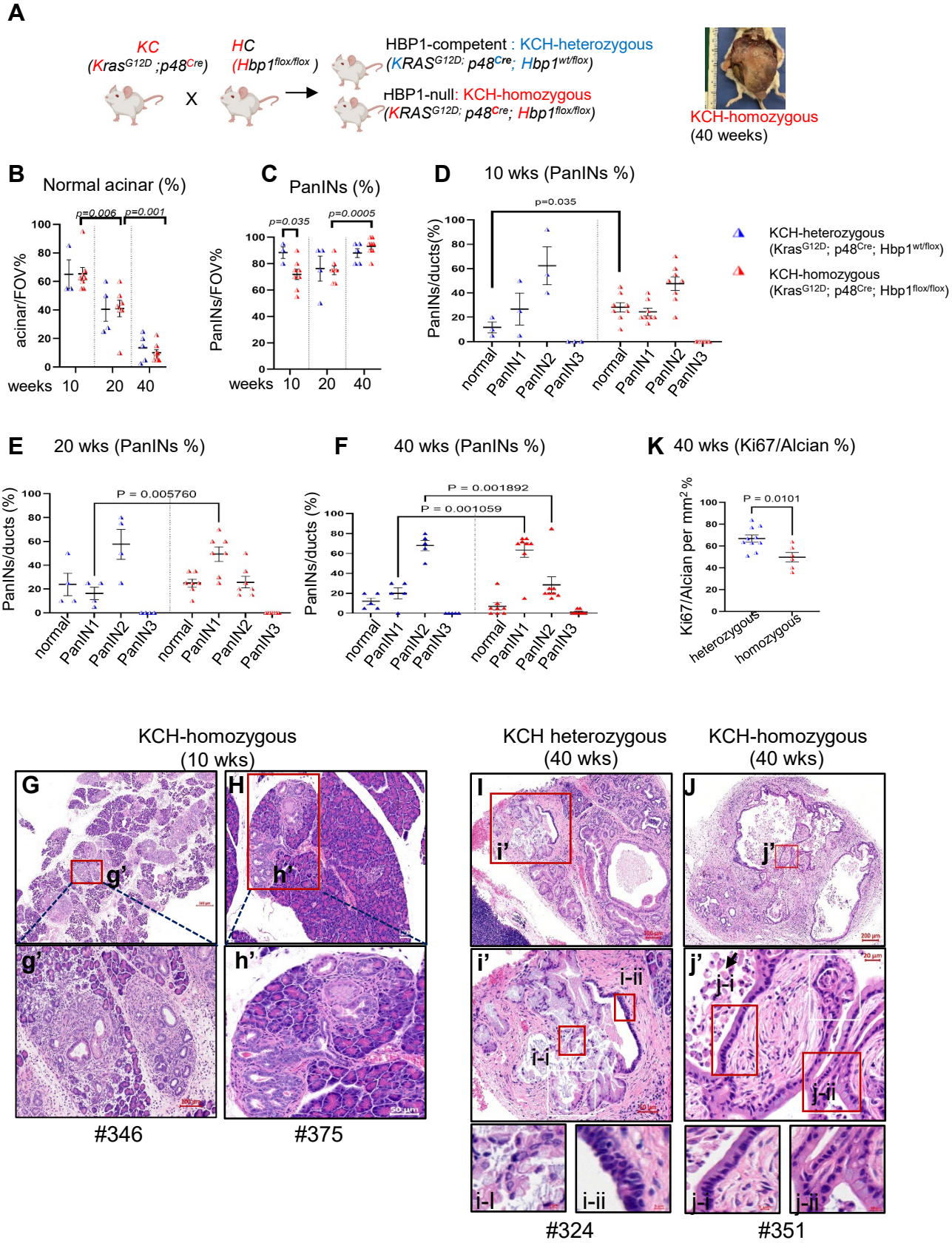

Lee & Ekstrom/Kim al.,2024

Figure S1

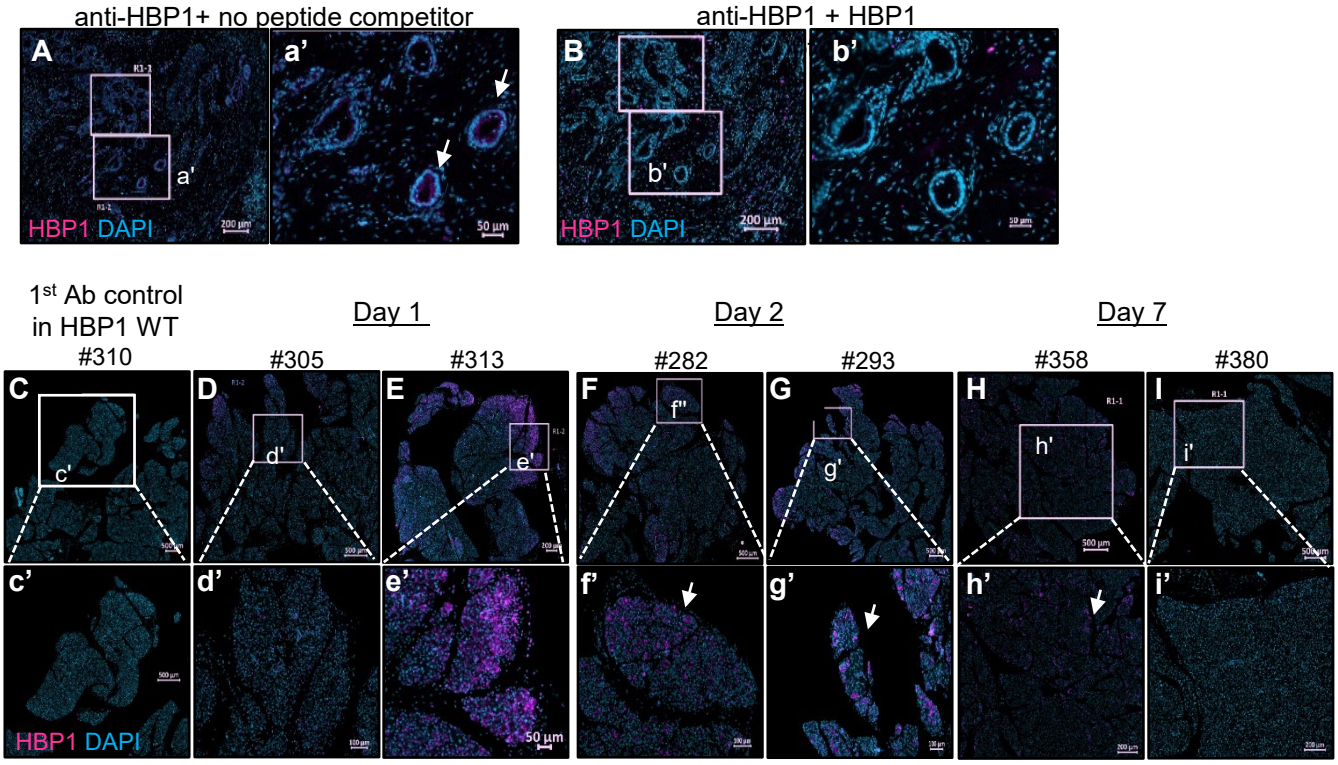

J. the fitted logistic regression models for combined cell types

	Estimate	Std. Error	Z value	p-val (>|Z|)
Intercept	1.08	0.85	1.27	0.2
HBP1 in acinar	-0.73	0.55	-1.34	0.18
HBP1 in duct	1.03	0.82	1.25	0.21
HBP1 in fibroblast	-133.49	54.85	-2.43	0.02

K. the fitted logistic regression models for each cell type

	Estimate	Std. Error	Z value	p-val (>|Z|)
Intercept	-0.01	0.47	-0.03	0.98
HBP1 in acinar	-0.94	0.49	-1.91	0.05

	Estimate	Std. Error	Z value	p-val (>|Z|)
Intercept	-1.23	0.53	-2.3	0.02
HBP1 in ductal	0.85	0.68	1,26	0.21

	Estimate	Std. Error	Z value	p-val (>|Z|)
Intercept	1.09	0.69	1.58	0.11
HBP1 in fibroblast	-132.99	52.17	-2.55	0.01

Lee & Ekstrom/Kim al.,2024
Figure S2

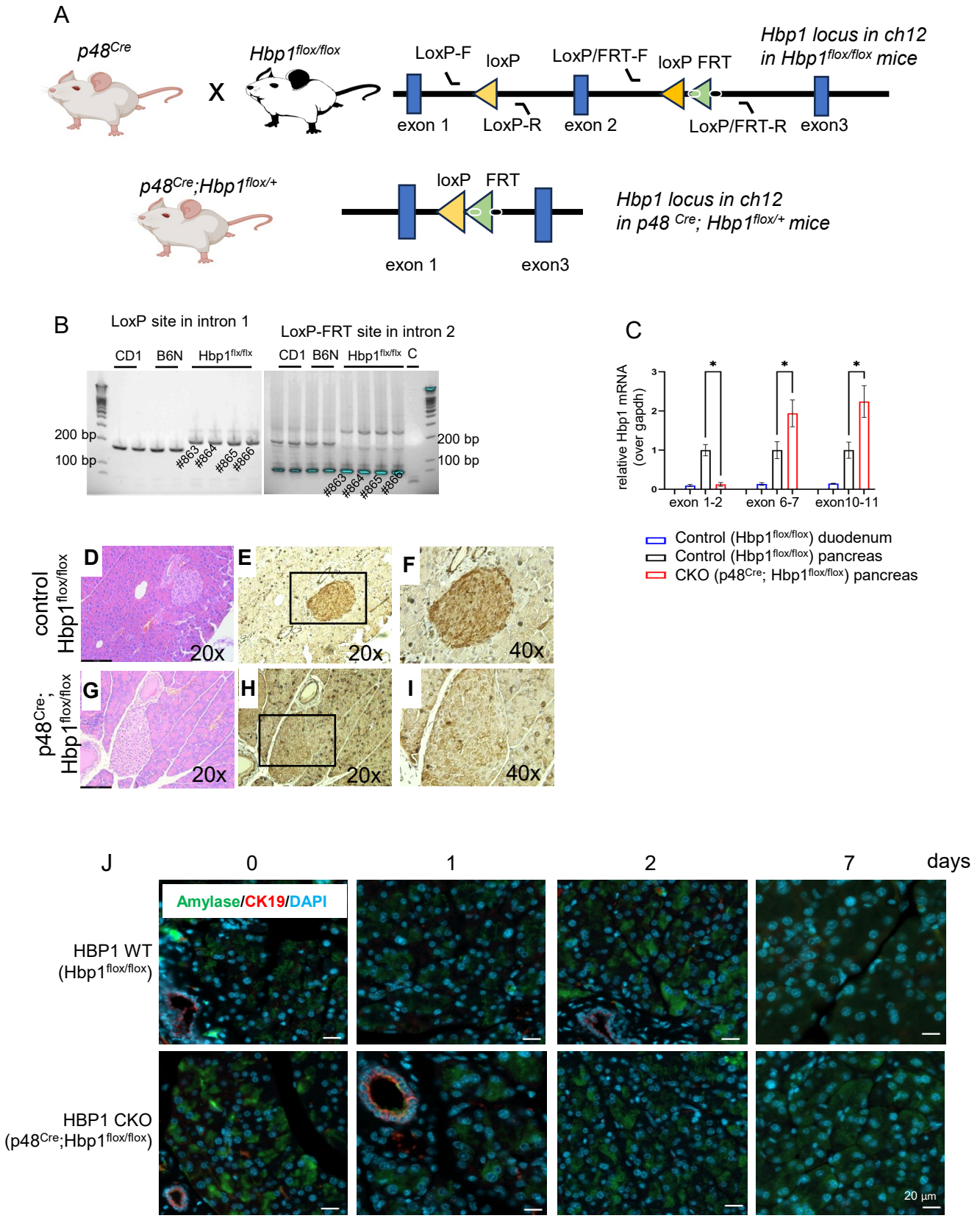

Lee & Ekstrom/Kim al.,2024

Figure S3

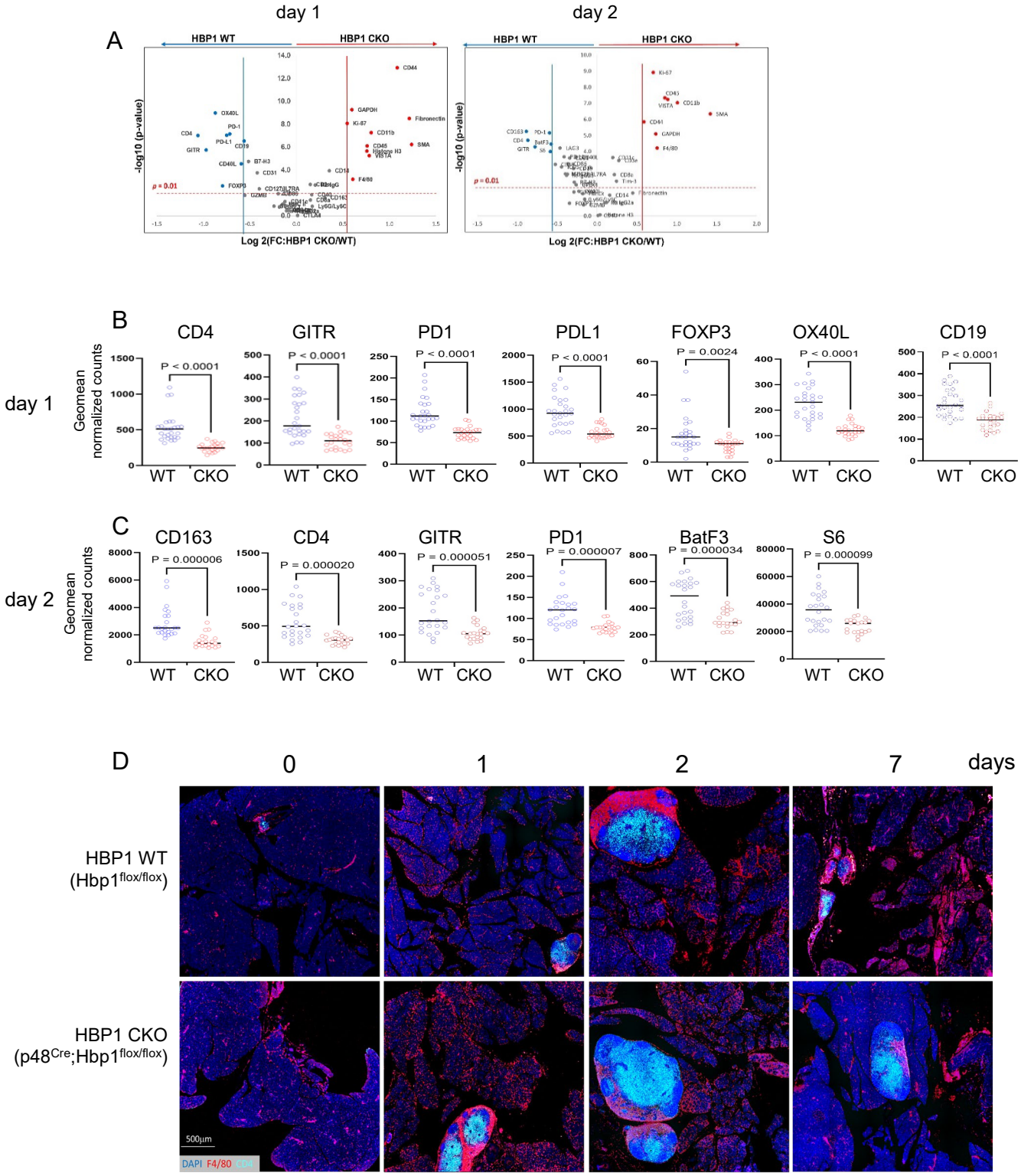

Lee & Ekstrom/Kim al.,2024
Figure S4

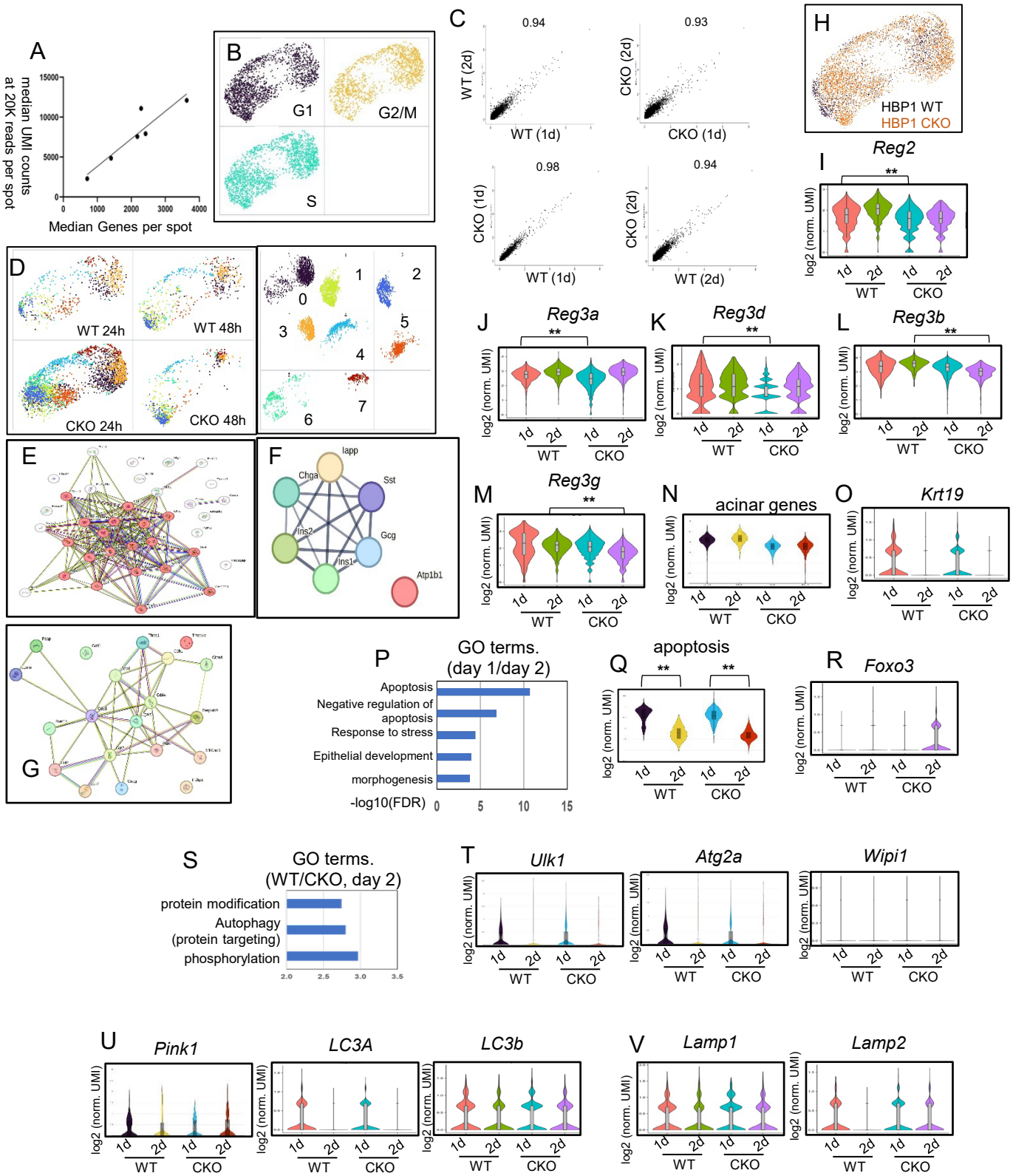

Lee & Ekstrom/Kim al.,2024
Figure S5

A. Diagram of inducible HBP1 (iHBP1) OE vector

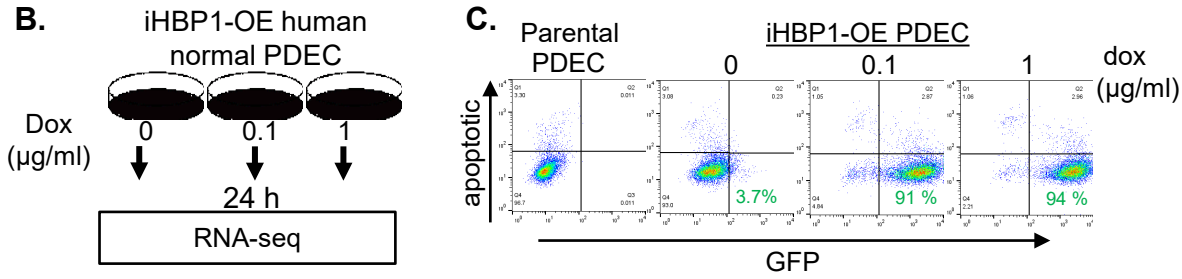

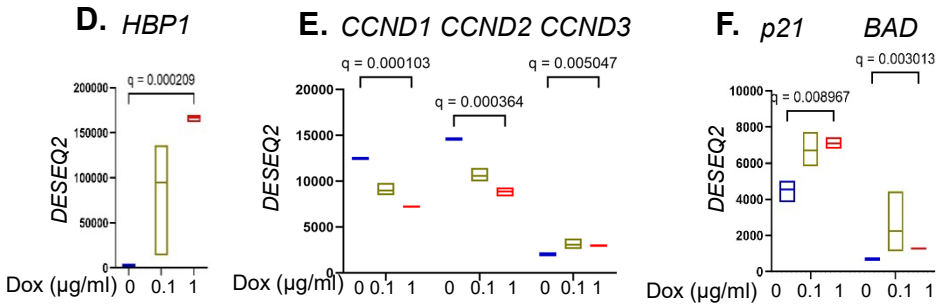

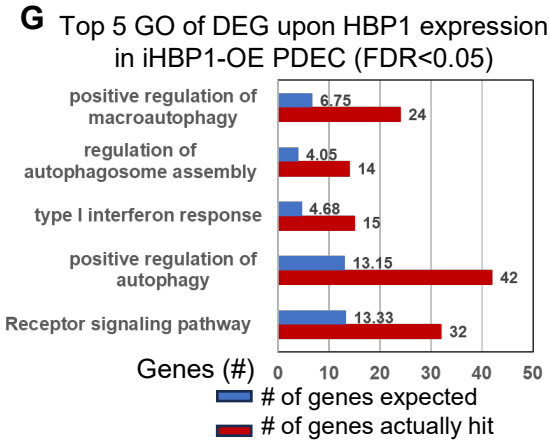

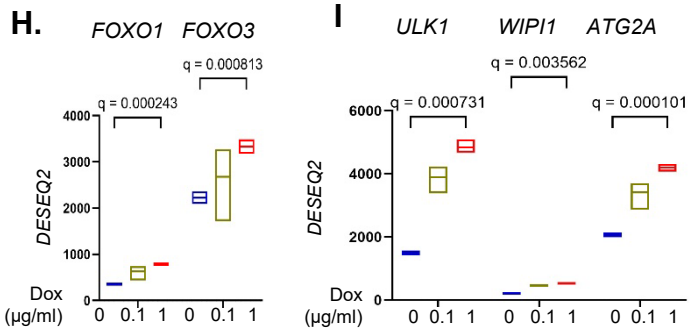

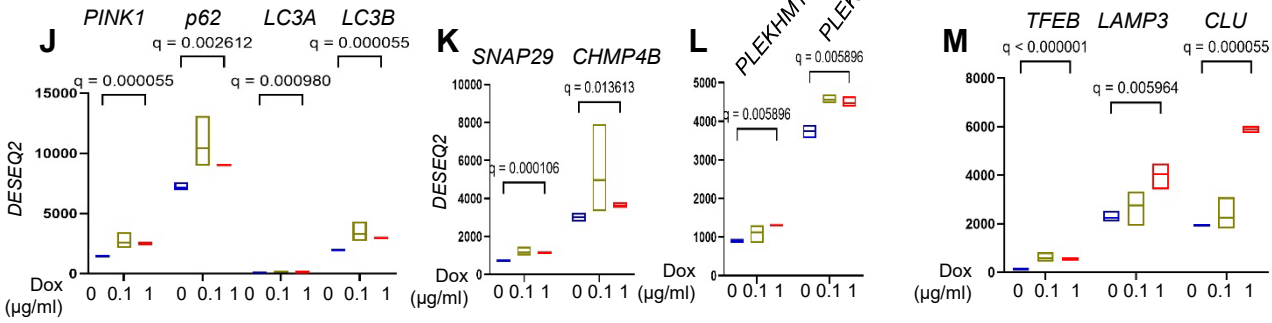

Lee & Ekstrom/Kim al.,2024
Figure S6

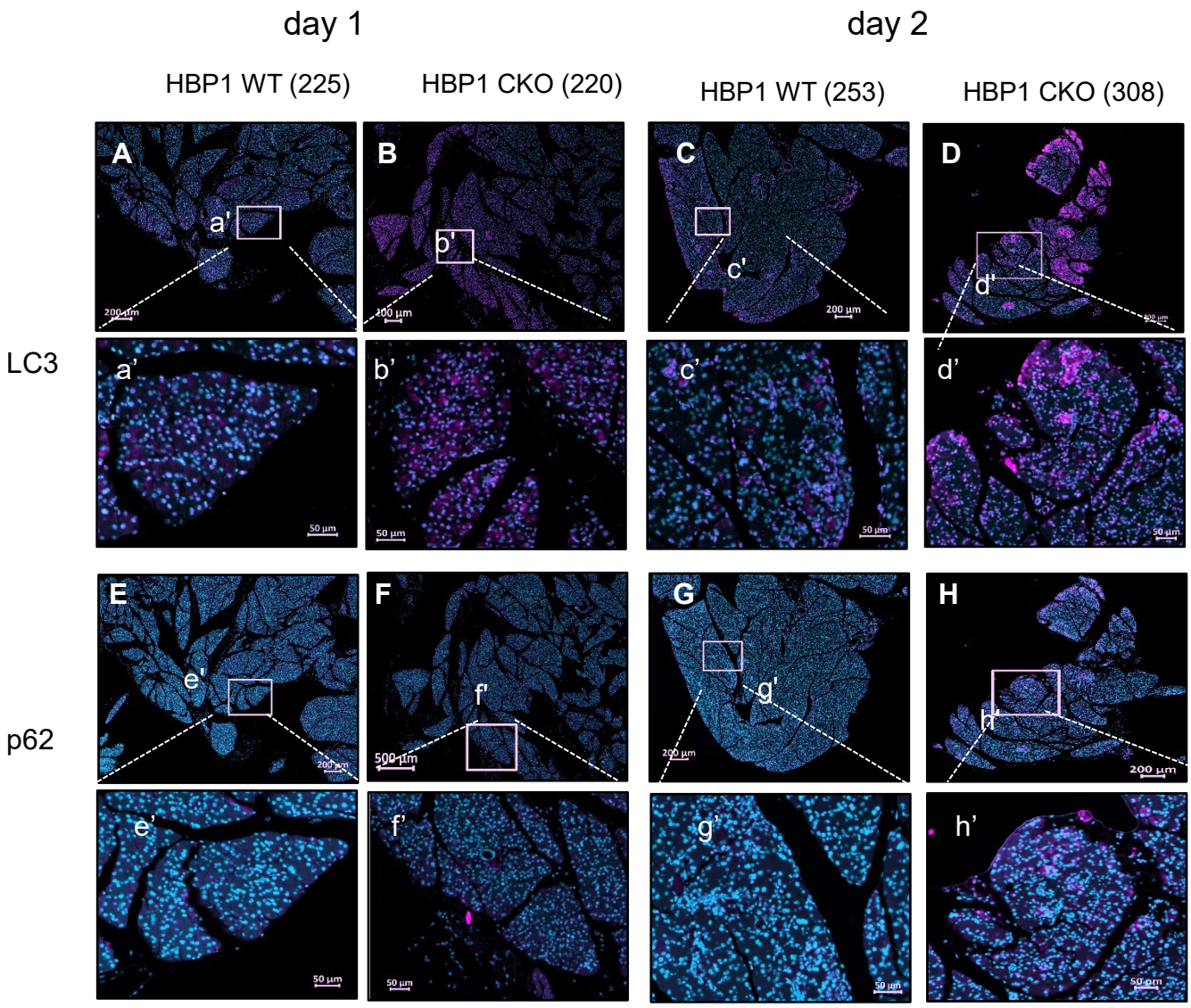
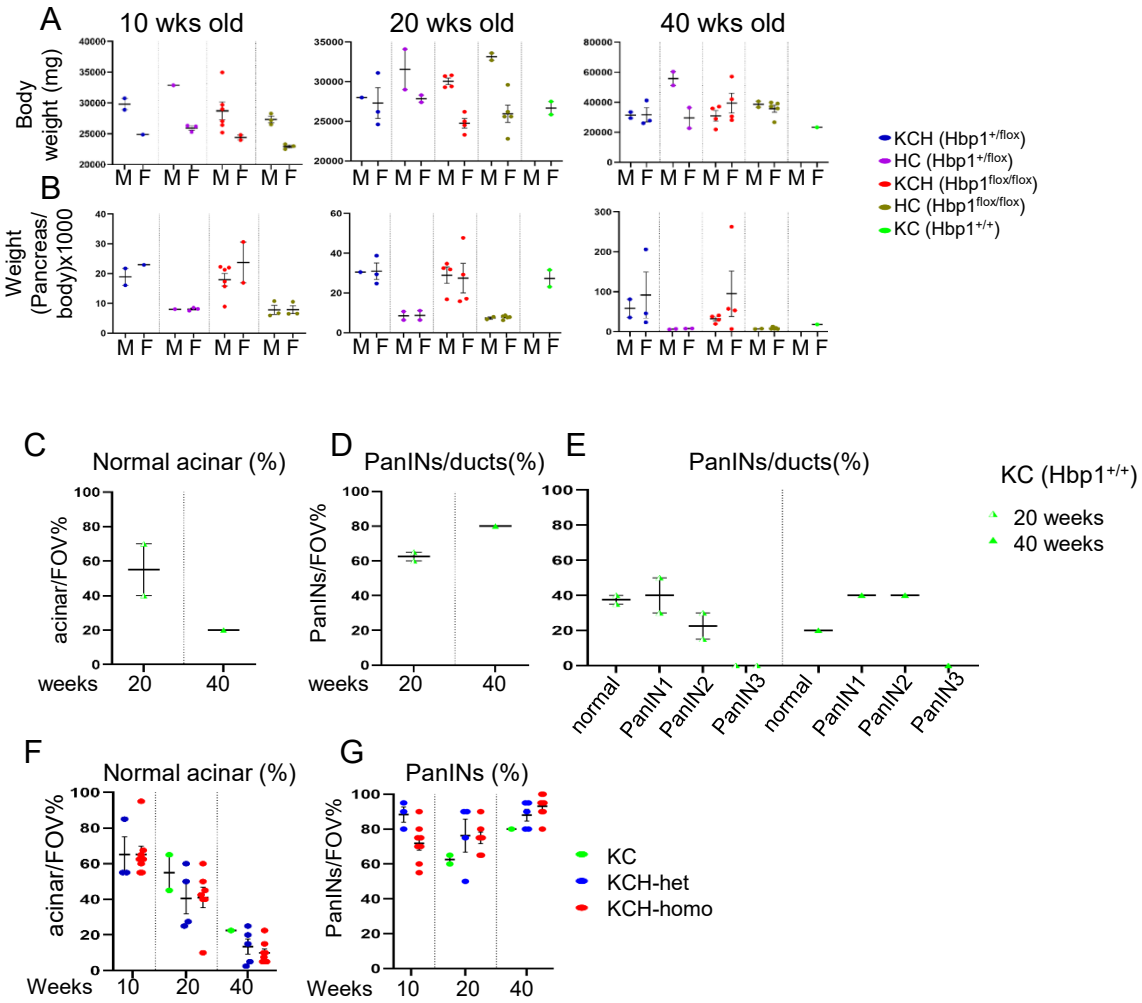
Lee & Ekstrom/Kim al.,2024
Figure S7